UNIVERSITY OF CALIFORNIA, DAVIS

BERKELEY • DAVIS • IRVINE • LOS ANGELES • MERCED • RIVERSIDE • SAN DIEGO • SAN FRANCISCO SANTA BARBARA • SANTA CRUZ

COLLEGE OF ENGINEERING

DEPARTMENT OF CIVIL & ENVIRONMENTAL ENGINEERING
ONE SHIELDS AVENUE
DAVIS, CALIFORNIA 95616
PHONE (530) 752-8180
FAX (530) 752-7872

1 November 2019

Dear Dr. Shiraiwa,

Below please find our point-by-point responses to the reviewers, along with a tracked changes version of our manuscript. The reviewers raised important points regarding data quality and potential measurement biases. We have considered these issues thoroughly and concluded that our measurements are robust . We have modified our manuscript accordingly.

Should you require further information or more detailed responses to help you make your decision we would be happy to provide.

Best regards,

Christopher D. Cappa
Ray B. Krone Professor of Environmental Engineering

Response to Reviewer #1

We thank the reviewer for the thoughtful comments. The reviewer raises as a primary concern the measurements of the small absorption enhancement observed at 781 nm and the relationship with the coating-to-core ratio for BC-containing particles, positing that there may be some measurement bias that is leading to a strong deviation from the core-shell behavior. Our responses are in **blue** and the initial reviewer comments in **black**.

General comments: The authors have comprehensively investigated the microphysical and optical properties of primary carbonaceous particles derived from various types of biomass-burning and their empirical relationships with some bulk parameters such as MCE and OA/BC ratio, on the basis of fire-chamber experiments. These results will be useful as a basis for interpreting the field-campaign data and for parameterization of size distribution and absorbing properties of OA, BrC, BC for biomass-burning plumes. The manuscript is logically written and display items are all easy to understand. How- ever, I have a serious concern in the author's interpretation of their experimental results as detailed below. I can recommend publication of this manuscript after the authors convincingly address this issue.

The primary argument provided by the reviewer is that the SP-AMS might be biased because coatings may not effectively vaporize if they are not engulfing the BC. Certainly this is a possibility. However, we note that if this occurred it would lead to a negative bias and thus the reported coating-to-core ratios would be a lower bound. This would seem to go opposite to the reviewers concern; if the actual coating-to-core ratios were even larger than reported then the disparity only increases. It is true that there is a differential sensitivity of the SP-AMS to BC compared to coating materials owing to how the particle beam overlaps with the laser beam in the instrument (Willis et al., 2014). However, this is more important for absolute quantification than it is for relative quantification (i.e., coating-to-core ratios). Based on Willis et al. (2014), if no accounting of the coating dependence of the detection were accounted for, such detection issues could lead to a bias of ca. 30% in the coating-to-core ratios. While important, such a bias would not materially affect the conclusions here.

We also note that there is an abundance of evidence in the literature for non-core-shell morphologies for fresh biomass-derived BC-containing particles. A just published paper from Adachi et al. (2019) shows images of BC attached to other material, consistent with some of their previous work (Adachi and Buseck, 2008;Adachi et al., 2010;Adachi and Buseck, 2011) and with various other similar measurements (Chakrabarty et al., 2006;China et al., 2013;Torvela et al., 2014). Using an SP2, Sedlacek et al. (2012) observed evidence of non-core-shell morphologies for BC-containing particles in a biomass burning plume, with the fraction of such particles >60% even in a somewhat aged plume. Also with an SP2, (Pan et al., 2017) observed fresh biomass combustion-derived large BC, averaged over many different fuel types and for large (>200 nm diameter) BC cores, exhibits a wide range of estimated shell-to-core diameter ratios and "delay times" that correspond to coating-to-core mass ratios of ca. 0.1 to 3.

One might ask why BC-containing particles from biomass combustion would not readily adopt core-shell morphologies, as the above cited experimental evidence suggests? We suggest BC and coating material existing in the same particles most likely results from near-source coagulation. Sedlacek et al. (2015) observed formation of non-core-shell morphologies from coagulation, albeit not for biomass burning derived particles.

Additionally, it should be considered that the SP-AMS coating-to-core ratios reported here are bulk averages and do not account for the different mixing states of BC-containing particles. The distribution of coating material across the population of particles impacts the absorption enhancement, even when core-shell morphologies are assumed (Fierce et al., 2016). This was also shown in Cappa et al. (2012) for a simple 1:1 bimodal mixture of a mode having smaller coating-to-core ratios (1 or 0.1) and one having values that allowed for matching of the observed coating-to-core ratio. For mixtures of this sort, the predicted absorption enhancement is smaller than obtained if all particles are assumed equivalent. Thus, the issue is not simply one of morphology, but of particle-to-particle mixing state.

Major critical comment: The authors observed the MAC_BC at 781 nm was nearly in- dependent of Rcoat_BC. And they just mentioned that this negligible coating-induced absorption enhancement of BC was consistent with previous results by McMeeking et al. (2014), without providing detailed physical interpretations. To my intuition, the coating-induced enhancement for an absorbing core embedded inside a non-absorbing host particle is a general consequence of electromagnetics law (i.e., Maxwell equation), and should not be violated excepting very rare cases (I don't know any example of such cases). One possible condition potentially consistent with the negligible enhancement is that the measured rBC-containing aerosols are in the morphological form of "attached-type" rather than "coated-type". However, the attached-type assumption seems to be inconsistent with the principle of coating measurement using the SP-AMS, because the coating materials on rBC may not effectively vaporize in that type. The authors should provide convincing theoretical discussion supporting the author's as- sumption that the observed negligible coating-induced enhancement is a real physical phenomenon (and not a consequence of some measurement artifacts). In this paper, a convincing interpretation of the negligible coating-induced enhancement is also needed for supporting the robustness of the BrC estimate according to Eq.(6).

The reviewer asks for "convincing theoretical discussion." We lack sufficient information regarding the mixing state (i.e., the distribution of coatings with respect to the BC particle population) and internal morphology to robustly calculate theoretical absorption enhancements for our experiments. However, example calculations following the approach of Cappa et al. (2012) can give an indication of what conditions might give rise to limited absorption enhancements, even at relatively large bulk-average coating-to-core ratios. Theoretical absorption enhancements, assuming core-shell morphologies, have been calculated for a binary population of particles, with one population "thinly" coated (with coating-to-core = 0.1) and one "thickly" coated (with variable coating-to-core ratios). The fraction of thickly coated particles (f_{thick}) was varied from 1 (for which the thickly coated coating-to-core ratio equals the bulk average) to 0.01. We have assumed a BC core diameter of 150 nm with a complex refractive index of 2.0 + 1.0*i*. The complex RI for the coating was assumed as $1.5 + 10^{-8}i$. The absorption enhancement was calculated for each assumed f_{thick} as a function of the bulk-average coating-to-core ratio. The results of these calculations are compared with the observations in Fig. 1a, and the variation in E_{abs} with the f_{thick} for three different bulk-average $R_{coat\text{-}BC}$ values (= 1, 5, and 10) are shown in Fig. 1b. These example calculations indicate that when the population is skewed towards most particles being thinly coated the theoretical E_{abs} can be quite small even when the bulk-average $R_{coat\text{-}BC}$ is large. We note again that these calculations assume a core-shell morphology, so deviations from core-shell would serve to reduce these values further, that is the calculations here are upper-limits. Measurements by Liu et al. (2017) indicate that the core-shell approximation fails for particles having coating-to-core ratios < 3, and even above this value there may still be reductions owing to non-core-shell morphologies. Further, we have considered only a simple binary mixture of thinly and thickly coated particles. Consideration of more complex distributions of material across the BC population would lead to further reductions in the calculated absorption enhancements.

All this is to say that there is a strong experimental and theoretical foundation for observing absorption enhancements lower than the core-shell approximation. Given the simplistic nature of the calculations presented here, the assumptions that go into them, and a lack of experimental constraints regarding the particle mixing state for the particles sampled, we hesitate to add too much of this discussion to the manuscript. Nonetheless, in the revised version we intend to expand somewhat the discussion on Page 10 where we already indicated that the relatively low and constant E_{abs} at 781 nm likely results from a combination of mixing state and morphology effects.

The reviewer also raises the question of whether the coating material vaporizes efficiently in the SP-AMS laser if the particles have an "attached-type" internal morphology. We, unfortunately, do not have evidence indicating whether such particles are or are not accurately characterized. However, we can consider what the impact would be on our results if this were a major issue. The reviewers concern seems to be that the coating material would be missed in the SP-AMS, although the rBC material should be detected. If this occurred, the bulk-average coating-to-core ratio observed would be underestimated. If this bias occurs (and again, we do not have evidence to argue one way or another whether it is a concern) then our coating-to-core estimates would be biased low, making the apparent gap between the core-shell expectation and the observed behavior even greater. Overall we agree with the reviewers comment that the presence of attached-type particles could contribute to the lower than expected enhancements, and imply as such when we stated that "Most likely, this lack of a substantial coating-induced enhancement results from a non-even distribution of non-BC mass across the population of BC particles (Fierce et al., 2016;Liu et al., 2017) and from the morphology of BC-containing particles not conforming to an idealized core-shell structure (Adachi et al., 2010).,

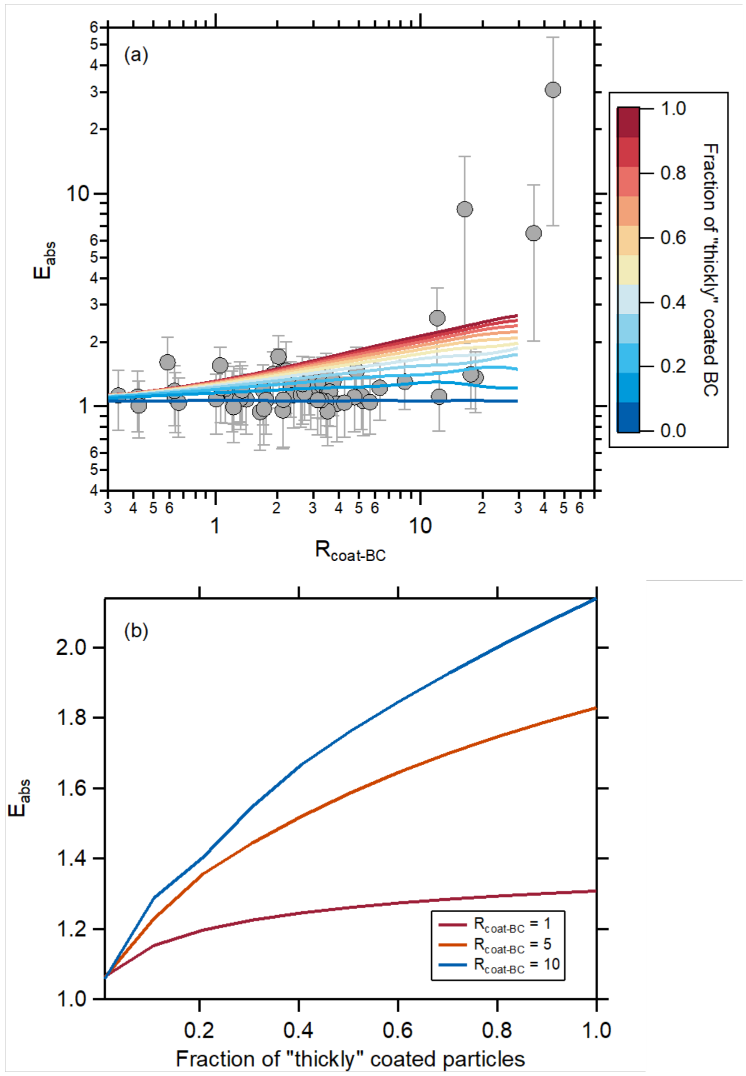

Figure 1. (a) The observed (points) absorption enhancement at 781 nm, calculated as the observed mass absorption coefficient divided by the reference value at the limit of no coating, and the calculated (lines) absorption enhancements from core-shell Mie theory as a function of the coating-to-core ratio. The different color lines correspond to different assumptions regarding the fraction of “thickly” coated BC. (b) The calculated absorption enhancement from core-shell Mie theory as a function of the fraction of “thickly” coated particles for three different bulk-average coating-to-core ratios.

References

Adachi, K., and Buseck, P. R.: Internally mixed soot, sulfates, and organic matter in aerosol particles from Mexico City, Atmospheric Chemistry and Physics, 8, 6469-6481, 2008.
Adachi, K., Chung, S. H., and Buseck, P. R.: Shapes of soot aerosol particles and implications for their effects on climate, J. Geophys. Res., 115, D15206, https://doi.org/10.1029/2009jd012868, 2010.
Adachi, K., and Buseck, P. R.: Atmospheric tar balls from biomass burning in Mexico, Journal of Geophysical Research-Atmospheres, 116, 7, https://doi.org/10.1029/2010jd015102, 2011.
Adachi, K., Sedlacek, A. J., Kleinman, L., Springston, S. R., Wang, J., Chand, D., Hubbe, J. M., Shilling, J. E., Onasch, T. B., Kinase, T., Sakata, K., Takahashi, Y., and Buseck, P. R.: Spherical tarball particles form

through rapid chemical and physical changes of organic matter in biomass-burning smoke, Proceedings of the National Academy of Sciences, 201900129, https://doi.org/10.1073/pnas.1900129116, 2019.
Cappa, C. D., Onasch, T. B., Massoli, P., Worsnop, D., Bates, T. S., Cross, E., Davidovits, P., Hakala, J., Hayden, K., Jobson, B. T., Kolesar, K. R., Lack, D. A., Lerner, B., Li, S. M., Mellon, D., Nuaanman, I., Olfert, J., Petaja, T., Quinn, P. K., Song, C., Subramanian, R., Williams, E. J., and Zaveri, R. A.: Radiative absorption enhancements due to the mixing state of atmospheric black carbon, Science, 337, 1078-1081, https://doi.org/10.1126/science.1223447, 2012.
Chakrabarty, R. K., Moosmüller, H., Garro, M. A., Arnott, W. P., Walker, J., Susott, R. A., Babbitt, R. E., Wold, C. E., Lincoln, E. N., and Hao, W. M.: Emissions from the laboratory combustion of wildland fuels: Particle morphology and size, Journal of Geophysical Research: Atmospheres, 111, D07204, https://doi.org/10.1029/2005jd006659, 2006.
China, S., Mazzoleni, C., Gorkowski, K., Aiken, A. C., and Dubey, M. K.: Morphology and mixing state of individual freshly emitted wildfire carbonaceous particles, Nat Commun, 4, https://doi.org/10.1038/ncomms3122, 2013.
Fierce, L., Bond, T. C., Bauer, S. E., Mena, F., and Riemer, N.: Black carbon absorption at the global scale is affected by particle-scale diversity in composition, Nat. Comm., 7, https://doi.org/10.1038/ncomms12361, 2016.
Liu, D. T., Whitehead, J., Alfarra, M. R., Reyes-Villegas, E., Spracklen, D. V., Reddington, C. L., Kong, S. F., Williams, P. I., Ting, Y. C., Haslett, S., Taylor, J. W., Flynn, M. J., Morgan, W. T., McFiggans, G., Coe, H., and Allan, J. D.: Black-carbon absorption enhancement in the atmosphere determined by particle mixing state, Nat. Geosci., 10, 184-U132, https://doi.org/10.1038/ngeo2901, 2017.
Pan, X., Kanaya, Y., Taketani, F., Miyakawa, T., Inomata, S., Komazaki, Y., Tanimoto, H., Wang, Z., Uno, I., and Wang, Z.: Emission characteristics of refractory black carbon aerosols from fresh biomass burning: a perspective from laboratory experiments, Atmos. Chem. Phys., 17, 13001-13016, https://doi.org/10.5194/acp-17-13001-2017, 2017.
Sedlacek, A. J., Lewis, E. R., Kleinman, L., Xu, J., and Zhang, Q.: Determination of and evidence for non-core-shell structure of particles containing black carbon using the Single-Particle Soot Photometer (SP2), Geophysical Research Letters, 39, n/a-n/a, https://doi.org/10.1029/2012GL050905, 2012.
Sedlacek, A. J., Lewis, E. R., Onasch, T. B., Lambe, A. T., and Davidovits, P.: Investigation of Refractory Black Carbon-Containing Particle Morphologies Using the Single-Particle Soot Photometer (SP2), Aerosol Science and Technology, 49, 872-885, https://doi.org/10.1080/02786826.2015.1074978, 2015.
Torvela, T., Tissari, J., Sippula, O., Kaivosoja, T., Leskinen, J., Virén, A., Lähde, A., and Jokiniemi, J.: Effect of wood combustion conditions on the morphology of freshly emitted fine particles, Atmospheric Environment, 87, 65-76, https://doi.org/10.1016/j.atmosenv.2014.01.028, 2014.
Willis, M. D., Lee, A. K. Y., Onasch, T. B., Fortner, E. C., Williams, L. R., Lambe, A. T., Worsnop, D. R., and Abbatt, J. P. D.: Collection efficiency of the soot-particle aerosol mass spectrometer (SP-AMS) for internally mixed particulate black carbon, Atmospheric Measurement Techniques, 7, 4507-4516, https://doi.org/10.5194/amt-7-4507-2014, 2014.

Response to Reviewer #2:

We thank the reviewer for the thoughtful comments regarding, among other issues, potential biases in the BC measurements and in the absorption measurements. Certainly such issues are important to consider. Below we provide a point-by-point response in which we argue that the potential issues raised by the reviewer did not impact our observations and that our interpretations are robust. Our responses are in **blue** and the initial reviewer comments in **black**.

1. First major concern is the source of black carbon (BC) constituting the Class 6 particles. Per table 1, the fuels burnt constitute duffs, peat, dung - all of which have been found to smolder (low MCE values) and produce tar-balls or spherical brown carbon (BrC) aerosol with negligible/no BC, very high SSA, and AAE >6 in the 405-532 nm. For example: Chakrabarty et al. ((2010), ACP 10, 6363) observed and reported no BC from duff burning at Missoula FSL. More recently, peat collected from Alaska and In- donesia were burned in a Missoula FSL-replica chamber (Sumlin et al. 2017 and 2018 series of papers) and negligible BC was found. These fuels have been only observed to smolder (low-temperature fires) both in the lab as well in field. Consequently, the particle formation mechanism is distinct in these fires, meaning soot (BC) formation is not supported.

Response: The reviewer here is arguing that there is zero BC produced. Later (Comments 4) the reviewer questions whether the OA can be absorbing at 781 nm and suggests that there is a more notable enhancement of BC absorption at 781 nm at very large Rcoat values. We find these arguments to be somewhat inconsistent. The very large Rbc values are determined for the systems where the total [OA]/[BC] ratios are largest. These correspond to the much more smoldering burns. If there is no BC (as the reviewer suggests) then there can be no enhancement of BC absorption and, related, if the OA is not absorbing then there should be no absorption at all if there is no BC. Yet, we clearly observe absorption at 781 nm for the high [OA]/[BC] systems (i.e., Class 6). Thus, we must conclude that, at minimum, there is either some small amount of BC for the Class 6 particles or the OA is somewhat absorbing at 781 nm. We believe our results suggest both to be true.

First, where the reviewer writes that Chakrabarty et al. (2010) "observed and reported no BC from duff burning," we note that the cited paper states only that "A statistically relevant number of particles have been examined for morphology using SEM, and it was found that a high fraction (>95%) of all particles from each of the three samples were tar balls." It is not stated what the other 5% of particles corresponded to. It is stated that thermal EC was measured for these same samples but "below detection limit." However, this is, perhaps, not unexpected given that the total OA/BC mass ratios we derived were larger than 1000 for these very OA-rich particles. The amount of BC (or EC) is indeed, quite small, and depending on the detection limit of the OC/EC instrument used any EC present might not be quantified. Further, one would need fewer than 1 in 1000, or even 1 in 10,000, particles to be BC (assuming the same mass-per-particle) for our results to hold. The total number of particles analyzed by Chakrabarty et al. (2010) was not reported, but we believe it quite reasonable to think that 1 in 1,000 particles could have been BC-containing. Additionally, we note that the analysis of Chakrabarty et al. (2010) shown in Fig. 4 and Eqn. 3 seems to implicitly assume that there is a BC contribution, which they note resulted from "minor flaming combustion during the ignition of the fire." Looking additionally to

Chakrabarty et al. (2016), who characterized emissions from Alaskan and Siberian peat, their Table 1 explicitly shows that BC is emitted. They report BC emission factors of 0.1-0.2 g kg^{-1} fuel, compared to OC emission factors of 4-7 g kg^{-1} fuel, corresponding to OA-to-BC ratios (assuming an OA/OC ratio of 1.6) of 32-176, which are smaller even than what we report. (We note that the actual results reported in Chakrabarty et al. (2016) contrasts with what is stated in Sumlin et al. (2017) where Sumlin (2017) state that for Chakrabarty (2016) "smoldering Alaskan and Siberian peat emissions contain BrC aerosols with no BC component.") There are also the results of Bhattarai et al. (2018), who characterized smoke from combustion of three different peats. They used EC/OC analysis for EC concentrations, and a PASS-3 for absorption. The EF's for EC are small (0.01-0.1 mg/g fuel), with OA/EC ratios of 154-522 (again assuming OA/OC = 1.6). Again, the amount of EC emitted is small, but not zero. For comparison, the [OA]/[BC] ratios we determined are even larger than this. The reviewer notes that Sumlin et al. (2017,2018) found "negligible" BC; it is not clear to us where this conclusion arises from since the reported measurement suite in Sumlin et al. (2017, 2018) did not include instrumentation for measurement of BC as best we can tell. Regardless, we are not arguing that there is a lot of BC here, and with an [OA]/[BC] > 1000 some might consider the amount of BC negligible. But, a "negligible amount" does not imply that BC is non-existent, and indeed there are literature results (e.g., Chakrabarty et al. (2016) and Bhattarai et al. (2018)) supporting the idea that there is a small amount of BC emitted from peat combustion.

Second, as to whether the OA is absorbing at 781 nm, we believe our observations are clear. If, as the reviewer contends, there is no BC present for these very OA-rich particles (which we do not think to be the case; see above) then there should be no absorption at 781 nm if they are not absorbing. Yet, the observed absorption at 781 nm was well above the detection limit. Thus, if there is no BC present the OA must be absorbing. (Also, if the OA is not absorbing at 781 nm, then the absorption at 1064 nm might be similarly small, and thus charring would not be expected.) But, as we argue, there is some small amount of BC present. Unless we are dramatically underestimating the amount of BC present in these very OA-rich particles then the magnitude of the derived MAC_BC values for these particular particles are too large (>100 m2/g in one case) to be reasonably explained through coating effects. Thus, again, the OA must be absorbing.

2. Could charring of organics by the SP2 and/or SP-AMS be responsible for enhanced rBC concentration erroneously showing up in particle classes, especially in Class 6? This needs to be addressed. Sedlacek et al. (Aerosol Research Letters 52:15, 1345- 1350) convincingly showed that initially near-IR transparent low-volatility compounds (fulvic and humic acid) particles at room temperature undergo chemical transformations as temperature is increased in a heated tube, creating new near-IR absorption transitions. They also say that this phenomenon enable SP2-induced charring of organic aerosol including tarballs (akin to Class 6 particles in this article). Sedlacek et al. observed around 5-10% mass loading of rBC in case of fresh OA/tar balls resulting from SP2-induced charring through near-IR light absorption. The reviewer is suspi- cious that the authors erroneously report rBC concentration corresponding to Class 6 particles due to this phenomenon and then draw their conclusions. Please provide substantive proofs that no soot photometer induced artifact is involved during the experiments, especially for Class 6 particles. If no evidence can be provided, please remove Class 6 particles from all plots which have [OA]/[BC] as the x-axis.

Response: The work of Sedlacek et al. (2018) is indeed important to consider. First, we believe it is very important to recognize that Sedlacek et al. (2018) only report that the SP2 detects fulvic acid and humic acid, BrC surrogates, as rBC when they are heated in a tube furnace to >500 degrees C. Their Fig. 2 shows that as this pre-heating temperature is reduced the likelihood of rBC detection is reduced. Indeed, it is implied in their paper (although not explicitly stated) that without heating neither fulvic acid or humic acid are detected as rBC in the SP2. In our experiments, the particles were not heated prior to detection with the SP2 (excluding the heating inherent in the particle generation). Thus, if our particles behave as fulvic or humic acid then we would not expect charring to be a concern.

Sedlacek et al. (2018) did also investigate charring of quite absorbing lab-generated tar balls, which is potentially of more relevance to our experiments than fulvic or humic acid samples. However, as they note "recent field observations suggest ambient tar balls may be less absorbing (*k* ~ 0.02i at 532 nm) than laboratory tar balls," with the latter having values around 0.2*i*. Our median derived MAC_{OA} at 532 nm was 0.21 m^2/g, corresponding to an imaginary RI of around 0.007*i*. Thus, our particles are more similar to field tar balls than lab-generated tar balls. Importantly, the tarballs investigated in Sedlacek et al. (2018) are not "akin to the Class 6 particles" as suggested by the reviewer. The reason for this is almost certainly the completely different particle production methods used in in our study versus by Sedlacek et al. (2018). Given the very different production methods, it is to be expected that the particle chemical properties differ, especially the graphitic content (which is likely of importance to any bias in the SP2 analysis).

3. The authors purport negligible absorption enhancement at 781 nm for Rcoat values as large as 10 based on results from Figure 4c. My concern with this assertion is that the axes in these graphs are extremely skewed which can misrepresent the actual MACBC enhancements. The average Eabs for Rcoat less than 10 is mentioned to be close to 1.2, but theoretical Eabs for longer wavelengths at these coating values are not expected to exceed 2 regardless (see Chakrabarty and Heinson, Phys. Rev. Lett., 2018). I believe that if the axes were not disproportionately skewed due to the extremely large MACBC values at the large OA/BC mass ratios (corresponding to Class 6 particles which in turn are due to the very small BC concentrations rather than large OA concentrations) we would be able to discern larger coating-induced absorption enhancements even at 781 nm. The conclusion that there is negligible coating-induced absorption enhancement based on visual comparison with a skewed axis is in my opinion is highly misleading. I notice that there are points in Fig 4c which have MACBC values larger than 10 which in turn would correspond to Eabs close to 2 which is significant in terms of absorption enhancements.

Recognizing the challenge of viewing things on multiple scales, we also included a version of this figure as Fig. S1, where results for each wavelength are shown on their own scale. We believe that there is also value in showing the results at the three different wavelengths on a common scale to visually illustrate the different behavior, and thus provided these two ways of viewing things. To the reviewers contention that we came to our conclusions based on "visual comparison with a skewed axis," this is simply not true. We came to our conclusion based on explicit calculation of the Eabs values from the observed MAC_{BC} values and the extrapolated value at zero coating and interrogation of these calculated values compared to the value determined from extrapolation to zero OA. As the reviewer notes, indeed there are MAC_{BC} values much larger than 10 in Fig. 4c at 781 nm. The reviewer implies that this results from a significant absorption enhancement. However, our observations are much more consistent with these large MAC_{BC} values resulting from OA absorption. As discussed above, even very weak absorption matters when the total [OA]/[BC] is large. This is why there is a much stronger relationship between the MAC_{BC} and the total [OA]/[BC] than there is with the [coating]/[BC] ratio. Further, we note that the largest MAC_{BC} values correspond to E_{abs} values > 10 (from MAC_{BC} values > 100 m^2/g). As the reviewer agrees, E_{abs} values from non-absorbing coatings on BC "are not expected to exceed 2". Thus, we must conclude that the observable enhancement includes an important contribution from BrC absorption. Finally, we note that if, as the reviewer contends above (although we disagree with), the [BC] are overestimated for Class 6 particles then the reported MAC_{BC} are underestimated for this class of particles, implying an even larger contribution from BrC. In any case, we have updated the manuscript to be more quantitative regarding the observed E_{abs} at 781 nm, adding the new text provided in our response to point 6 below.

4. The authors claim that the increased MACBC at 781 nm is due to OA absorption and not coating-induced. They need to cite relevant literature which demonstrates significant BrC absorption at longer wavelengths to back up this assertion.

While we believe our observations are clear on their own (see above discussion), we are happy to cite relevant literature. If the reviewer has any particular studies in mind, we would be happy to include them. Otherwise, we can include (for example) the classic paper of Kirchstetter et al. (2004), who report absorption by OC out to at least 700 nm, along with some others (Alexander et al., 2008;Phillips and Smith, 2017;Sengupta et al., 2018;Sumlin et al., 2018). We have added these to Table S3.

We also make the simple argument here: various studies indicate that absorption by BrC declines reasonably continuously with increasing wavelength. So, a thought experiment. If the $MAC_{OA405nm}$ = 1 m^2 g^{-1} and the AAE = 5, simple extrapolation (assuming a constant AAE) yields an $MAC_{OA,781nm}$ = 0.037 m^2 g^{-1}. This is small, but not zero and, when the OA concentration is much larger than the BC concentration, should be readily observable. If we instead assume the larger AAE values observed in our study, ~8.5, the extrapolated $MAC_{OA,781nm}$ = 0.01 m^2 g^{-1}. A key point is that when the OA abundance is sufficiently large even weak OA absorption can matter. This can be looked at one additional way. Consider that the absorption ratio between BC and OA is equal to ([BC]*MAC_{BC}/[OA]*MAC_{BrC}). If the [BC]/[OA] ratio is 10^{-3} (which we observe) then the OA absorption will be observable even if the ratio MAC_{BC}/MAC_{BrC} is 1000. Given an MAC_{BC} ~4 m^2/g at 781 nm, this means the MAC_{BrC} need only be 0.004 m^2/g to matter at the largest [OA]/[BC]. We contend it is quite reasonable to think that some BrC is at least this absorbing at 781 nm. Such exceptionally small absorption might be true for some secondary OA, it seems less likely for OA from biomass combustion, which typically has larger MAC_{OA} values compared to SOA (see Lambe et al. (2013)).

5. In Figure 4, it does not make sense to include points for MACBC where the contribution of BrC to total absorption is much larger than that of BC. So, removing all points for Class 6 OA would make the plots in Figure 4 more informative. The BC concentration in Class 6 is very likely an artifact. The absorption enhancement at longer wavelengths have a weaker dependence on coating thickness than at shorter wavelengths as ob- served by Pokhrel et

al. (2017) cited in the manuscript, but it is still significant. I am unconvinced of the insignificance of coating-induced BC light absorption enhancement asserted by the manuscript or at least from the results as they have been presented right now.

First, as we discuss extensively above, the BC concentration is Class 6 is not likely an artifact, and thus removal of these points is not warranted. Second, we wish to clarify that nowhere do we conclude that the absorption enhancement is “insignificant.” We did, however, state it is “negligible,” and we believe this consistent with our observations. Perhaps this is parsing words, but we believe there is a difference between “negligible” and “insignificant.” The median E_{abs} (based on the ratio of MAC_{BC} values), excluding the values that are exceptionally large (>3, and almost certainly dominated by OA absorption) was 1.14 and the mean was 1.17. These are “significantly” greater than one (in the statistical sense), yet still, in our view, “negligible.” However, we have revised the language in the paper to note that there is “only a minor coating-induced enhancement,” rather than a “negligible” enhancement and to make our statements more quantitative. Some of this was already discussed in Section 3.4.2, where we reported the mean E_{abs} at 781 nm. However, we have added an additional paragraph at the end of Section 3.4.1.

> “Values for the absorption enhancement at 781 nm are calculated as the ratio between the observed MAC_{BC} in **Figure 4** and the derived $MAC_{BC,pure}$. The derived E_{abs} range from 0.96 to 27. Values greater than two occur only for the particles having particularly large [OA]/[BC], > 400. As E_{abs} values much greater than two at 781 nm are unlikely to result from mixing-induced enhancements, this again suggests that the OA is somewhat absorbing at this wavelength. For the burns where [OA]/[BC] < 400, the median E_{abs} = 1.14 and the arithmetic mean E_{abs} = 1.19 ± 0.14 (1σ). Given that some of this enhancement may result from BrC absorption at 781, these values can be considered upper-limits on $E_{abs,coat}$, and the small magnitude is consistent with our conclusion above that, while likely greater than zero, the mixing-induced enhancement is generally negligible. It is possible that the $E_{abs,coat}$ values when [OA]/[BC] > 400 are substantially larger. However, given the general lack of a dependence of the $MAC_{BC,781nm}$ for $R_{BC\text{-}coat}$ < 10 this seems unlikely.”

Alexander, D. T. L., Crozier, P. A., and Anderson, J. R.: Brown Carbon Spheres in East Asian Outflow and Their Optical Properties, Science, 321, 833-836, https://doi.org/10.1126/science.1155296, 2008.

Bhattarai, C., Samburova, V., Sengupta, D., Iaukea-Lum, M., Watts, A. C., Moosmuller, H., and Khlystov, A. Y.: Physical and chemical characterization of aerosol in fresh and aged emissions from open combustion of biomass fuels, Aerosol Science and Technology, 52, 1266-1282, https://doi.org/10.1080/02786826.2018.1498585, 2018.

Chakrabarty, R. K., Moosmüller, H., Chen, L. W. A., Lewis, K., Arnott, W. P., Mazzoleni, C., Dubey, M. K., Wold, C. E., Hao, W. M., and Kreidenweis, S. M.: Brown carbon in tar balls from smoldering biomass combustion, Atmospheric Chemistry and Physics, 10, 6363-6370, https://doi.org/10.5194/acp-10-6363-2010, 2010.

Chakrabarty, R. K., Gyawali, M., Yatavelli, R. L. N., Pandey, A., Watts, A. C., Knue, J., Chen, L. W. A., Pattison, R. R., Tsibart, A., Samburova, V., and Moosmuller, H.: Brown carbon aerosols from burning of boreal peatlands: microphysical properties, emission factors, and implications for direct radiative forcing, Atmospheric Chemistry and Physics, 16, 3033-3040, https://doi.org/10.5194/acp-16-3033-2016, 2016.

Kirchstetter, T. W., Novakov, T., and Hobbs, P. V.: Evidence that the spectral dependence of light absorption by aerosols is affected by organic carbon, Journal of Geophysical Research-Atmospheres, 109, D21208, 2004.
Lambe, A. T., Cappa, C. D., Massoli, P., Onasch, T. B., Forestieri, S. D., Martin, A. T., Cummings, M. J., Croasdale, D. R., Brune, W. H., Worsnop, D. R., and Davidovits, P.: Relationship between Oxidation Level and Optical Properties of Secondary Organic Aerosol, Environmental Science & Technology, 47, 6349-6357, https://doi.org/10.1021/es401043j, 2013.
Phillips, S. M., and Smith, G. D.: Spectroscopic comparison of water- and methanol-soluble brown carbon particulate matter, Aerosol Science and Technology, 51, 1113-1121, https://doi.org/10.1080/02786826.2017.1334109, 2017.
Sedlacek, A. J., Onasch, T. B., Nichman, L., Lewis, E. R., Davidovits, P., Freedman, A., and Williams, L.: Formation of refractory black carbon by SP2-induced charring of organic aerosol, Aerosol Science and Technology, 52, 1345-1350, https://doi.org/10.1080/02786826.2018.1531107, 2018.
Sengupta, D., Samburova, V., Bhattarai, C., Kirillova, E., Mazzoleni, L., Iaukea-Lum, M., Watts, A., Moosmüller, H., and Khlystov, A.: Light absorption by polar and non-polar aerosol compounds from laboratory biomass combustion, Atmos. Chem. Phys., 18, 10849-10867, https://doi.org/10.5194/acp-18-10849-2018, 2018.
Sumlin, B. J., Pandey, A., Walker, M. J., Pattison, R. S., Williams, B. J., and Chakrabarty, R. K.: Atmospheric Photooxidation Diminishes Light Absorption by Primary Brown Carbon Aerosol from Biomass Burning, Environmental Science & Technology Letters, 4, 540-545, https://doi.org/10.1021/acs.estlett.7b00393, 2017.
Sumlin, B. J., Heinson, Y. W., Shetty, N., Pandey, A., Pattison, R. S., Baker, S., Hao, W. M., and Chakrabarty, R. K.: UV–Vis–IR spectral complex refractive indices and optical properties of brown carbon aerosol from biomass burning, Journal of Quantitative Spectroscopy and Radiative Transfer, 206, 392-398, https://doi.org/10.1016/j.jqsrt.2017.12.009, 2018.

Biomass-burning derived particles from a wide variety of fuels: Part 1: Properties of primary particles

Crystal D. McClure[1], Christopher Y. Lim[2,%], David H. Hagan[2], Jesse H. Kroll[2], Christopher D. Cappa[1,3,*]

[1] Department of Civil and Environmental Engineering, University of California, Davis, CA 95616
[2] Department of Civil and Environmental Engineering, Massachusetts Institute of Technology, Cambridge, MA, USA
[3] Atmospheric Sciences Graduate Group, University of California, Davis, CA, USA 95616
[%] Now at Department of Chemistry, University of Toronto, Ontario, Canada

[*] To whom correspondence should be addressed: cdcappa@ucdavis.edu

ABSTRACT

Relationships between various optical, physical, and chemical properties of biomass combustion derived particles are characterized for particles produced from a wide range of fuels and burn conditions. The modified combustion efficiency (MCE), commonly used to parameterize biomass particle emissions and properties, is shown to generally have weak predictive capabilities, especially for more efficient combustion conditions. There is, however, a strong relationship between many intensive optical properties (e.g. single scatter albedo, Ångstrom absorption exponent, mass absorption efficiency) and the organic aerosol-to-black carbon ([OA]/[BC]) mass ratio over a wider range than previously considered (0.3 to 10^5). The properties of brown carbon (BrC, i.e. light absorbing organic carbon) also vary with [OA]/[BC]. The contribution of coating-induced enhancements (i.e. "lensing" effects) to absorption by black carbon are shown to be negligible for all conditions. The BC-OA mixing state varies strongly with [OA]/[BC]; the fraction of OA that is internally mixed with BC decreases with [OA]/[BC] while the relative amount of OA coated on BC increases. In contrast, there is little relationship between many OA bulk chemical properties and [OA]/[BC], with the O:C and H:C atomic ratios and the relative abundance of a key marker ion (*m*/*z* = 60, linked to levoglucosan) all showing no dependence on [OA]/[BC]. In contrast, both the organic nitrate fraction of OA and the OA volatility do depend on the [OA]/[BC]. Neither the total particle or BC-specific size distributions exhibit any clear dependence on the burn conditions or [OA]/[BC], although there is perhaps a dependence on fuel type. Overall, our results expand on existing knowledge to contribute new understanding of the properties of particles emitted from biomass combustion.

1 Introduction

While it is understood that both open and controlled biomass combustion are major sources of particles to the atmosphere (Andreae and Merlet, 2001), questions remain regarding the properties of the emitted particles, their relationship with combustion conditions and fuel type, and their atmospheric evolution. Particles emitted from biomass combustion impact the global radiation budget and contribute to poor air quality in impacted regions. The emitted primary particles are primarily composed of organic aerosol (OA) and black carbon (BC), in varying amounts, with trace inorganic species (Reid et al., 2005;McMeeking et al., 2009;Levin et al., 2010). Particle intensive properties are often compared against the modified combustion efficiency (MCE ~ $\Delta[CO_2]/(\Delta[CO]+\Delta[CO_2])$), which provides a measure of the combustion efficiency of a burn. For example, various particle properties show some relationship with MCE, but often these relationships are weak, especially for more efficient combustion (higher MCE, corresponding typically to flaming conditions) (McMeeking et al., 2009;Liu et al., 2013;McMeeking et al., 2014). Understanding the diversity in the chemical, physical, and optical properties of the emitted particles is important for establishing the fire- or region-specific emissions and subsequent impacts.

The emitted OA from biomass combustion is somewhat light absorbing (Kirchstetter et al., 2004). Absorbing OA is commonly referred to as brown carbon (BrC), with properties that appear to depend on the fuel and combustion conditions (Saleh et al., 2014;Laskin et al., 2018), which affect particle organic composition (Jen et al., 2019). However, the properties of primary BrC absorption and, especially, understanding of the relationships between BrC absorption and other particle properties and burn conditions is only beginning to be unraveled. Additionally, it is established from theory and laboratory experiments that non-absorbing coatings on black carbon and other strongly absorbing particles can enhance the absorption (commonly referred to as the "lensing" effect but more accurately termed here the coating-induced enhancement) (Fuller et al., 1999;Bond et al., 2006;Lack et al., 2009;Shiraiwa et al., 2010;Cappa et al., 2012). Yet, the extent to which coating-induced enhancements impact absorption by ambient particles or for mixed-component particles from complex sources, such as biomass burning, remains contentious (Cappa et al., 2012;Healy et al., 2015;Liu et al., 2015;Peng et al., 2016;Liu et al., 2017).

Here, we expand on current understanding of the relationships between various primary particle properties and burn conditions by analyzing measurements of primary biomass burning particles produced from combustion of a variety of fuel types, many of particular relevance to the western U.S.. We demonstrate that various optical properties exhibit a strong relationship with the [OA]/[BC] mass ratio, much stronger than their relationship with the MCE. We use the measurements to quantify the individual contributions of BC, BrC and from internal mixing of BC to the observed light absorption, and examine the variability in the properties of BrC specifically. We uniquely characterize the mixing state of BC and OA, and how mixing state vary between individual burns and depend on the mean properties of the emitted particles. We characterize the variability of OA-specific properties, including OA volatility, bulk chemical composition (characterized by the O:C and H:C atomic ratio, and the presence of key marker ions), and, uniquely, the relative abundance of organic nitrate species. We also examine the variability in the emitted particle size distribution, both for the total particles and for the BC particles specifically. Some of our analysis serves to support and extend previously determined relationships by considering a wider range of conditions, while other aspects are unique to this study. These observations provide a foundation for understanding and interpretation of experiments on the influence of photochemical aging on biomass particle properties, discussed in a related paper (Lim et al., 2019).

Deleted: e

2 Methods

All experiments were conducted during the Fire Influence on Regional to Global Environments Experiment (FIREX) lab study, which took place at the Missoula Fire Sciences Lab in Missoula, MT, USA during November, 2016. Numerous types of biomass were combusted in a large chamber (12 x 12 x 19 m) and the smoke sampled to provide information on the physical, chemical, and optical properties of the resulting smoke (i.e., particulate and gas emissions). The general fuels types combusted included (exclusively or in combination): duff, dung, excelsior, straw, litter, untreated lumber, rotten debris, woody debris, shrub, herbaceous, and canopy biomass. A complete list of fuels and types is provided in **Table S1**, with further details available on the U.S. National Oceanic and Atmospheric Administration (NOAA) data archive (https://esrl.noaa.gov/csd/projects/firex/). All data used in this publication are also available on the NOAA archive, with the processed data summarized in complementary data repository (Cappa et al., 2019a).

Formatted: Font: Bold

Deleted: Table S1

Both “room” and “stack” burns were conducted, although here we include results only from stack burns. During stack burns, the smoke was mixed with background room air and funneled up a large cylindrical stack (2 m dia. x 15 m height) where it was sampled into a high-flow transfer line at ca. 0.27 m^3/s. This flow rate corresponded to sampling approximately 10% of the stack flow. Smoke was transferred to an adjacent room via the high-flow transfer line (residence time ca. 2 s) where it was sub-sampled through a $PM_{2.5}$ cyclone and injected into a 0.25 m^3 Teflon photochemical reaction chamber (the mini chamber). Details on the construction and operation of the mini chamber can be found in (Lim et al., 2019). Here, we focus exclusively on the properties of particles sampled prior to initiation of photochemical oxidation; results of the photochemical oxidation experiments are discussed in a series of papers (Coggon et al., 2019;Lim et al., 2019). In brief, prior to each burn, the chamber was flushed with clean air with a relative humidity (RH) of approximately 40%. To fill the chamber, smoke was sub-sampled from the high-flow inlet and injected across the entire burn (typically lasting for 10-20 minutes) or until the chamber concentration reached a maximum. A suite of instruments sampled from the mini chamber at a flow rate of approximately 6 lpm. This flow rate varied from burn to burn due to the exact suite of instruments sampling. Clean makeup air was being injected simultaneously from a zero air generator to equal the air being sampled out of the chamber. The sampled smoke was diluted by a factor of ca. seven relative to the air in the high-flow inlet. Subsequent dilution after filling was characterized by the decay of acetonitrile (ACN). Properties of the primary particles are averaged over the 5-10 minute period after filling but before the initiation of photochemistry.

Particle-phase instrumentation sampled alternatingly every two minutes through a thermodenuded or ambient sample line. The thermodenuder was operated at 300 ºC with a residence time of approximately 5 s and volatilized semi-volatile components, including those that are internally mixed with BC. The ambient line was lined with a charcoal cloth that removed excess gases (such as VOCs, NO_x, and O_3) that could interfere with particle-phase measurements. Comparison of thermodenuded versus ambient particles allowed for the investigation of coating amount and volatility. The gas-phase composition in the mini chamber was similar to that sampled directly from the fire (Koss et al., 2018;Lim et al., 2019). Particle phase instrumentation included: a multi-wavelength cavity-ringdown-photoacoustic absorption spectrometer (CRD-PAS) and a photoacoustic absorption spectrometer (PASS-3) for characterization of light absorption and extinction coefficients at 405 nm, 532 nm, and 781 nm; a high resolution aerosol mass spectrometer (HR-ToF-AMS) for characterization of non-refractory submicron particulate matter ($NR\text{-}PM_1$) components (i.e. OA, NO_3, SO_4, NH_4, Cl, K); a soot photometer AMS (SP-AMS) in laser-only mode for characterization of refractory BC and the NR-components that are internally mixed with BC; a single particle soot photometer (SP2) for characterization of refractory BC mass concentrations and size distributions; and a scanning electrical mobility sizer (SEMS) for measurement of particle mobility size distributions. Further details regarding instrument operation and calibration are provided in the Supplemental Material and in Lim et al. (2019).

3 Results and Discussion

3.1 Bulk optical property relationships

Due to the wide variety of biomass fuels and types used during FIREX, there was a substantial diversity in the properties of primary particles produced. Previous studies have shown both the single scatter albedo (SSA) and wavelength-dependence of absorption (the absorption Angstrom exponent, AAE) depend on the modified combustion efficiency (MCE) (Liu et al., 2013;McMeeking et al., 2014;Pokhrel et al., 2017). The MCE is defined here as:

$$\boldsymbol{MCE} = \frac{[\boldsymbol{CO_2}]}{[\boldsymbol{CO_2}]+[\boldsymbol{CO}]} \quad (1)$$

The SSA is defined as:

$$SSA = \frac{b_{ext}-b_{abs}}{b_{ext}} \quad (2)$$

where b_{ext} is the wavelength-specific extinction coefficient and b_{abs} is the wavelength-specific absorption coefficient. The AAE is defined as:

$$AAE = -\log\left(\frac{b_{abs,\lambda 1}}{b_{abs,\lambda 2}}\right) / \log\left(\frac{\lambda 1}{\lambda 2}\right) \quad (3)$$

where λ_1 and λ_2 indicate two different wavelengths, here 405 nm and 532 nm. The MCE characterizes the overall combustion efficiency, with values closer to unity indicating more complete combustion. In general, higher MCE correspond to more flaming combustion conditions while smaller MCE correspond to more smoldering conditions. We find a similar relationship between SSA_{405nm}, AAE, and [OA]/[BC] with MCE as previous studies (**Figure 1**) (McMeeking

Deleted: Figure 1

et al., 2009;Liu et al., 2013;McMeeking et al., 2014;Pokhrel et al., 2017). Specifically, the SSA_{405nm} is relatively constant and near unity for MCE < ~0.9, but above this value exhibits a rapid decline, albeit with a substantial amount of scatter (**Figure 1**a). The AAE is also relatively constant when MCE < 0.9, with very large values (AAE ~ 8). There is a rapid, scattered decrease in the AAE as MCE increases further (**Figure 1**b). The relationship between [OA]/[BC] and MCE is similar, with values generally decreasing as MCE increases but a large amount of scatter (**Figure 1**d). There is also a general relationship between the mass absorption coefficient referenced to BC (MAC_{BC}) at 405 nm and the MCE, but with similar scatter as the other properties (**Figure 1**c). The MAC_{BC} is defined as:

$$MAC_{BC} = b_{abs}/[BC] \quad (4)$$

The $MAC_{BC,405nm}$ includes contributions from absorption by BC, BrC, and from coating-induced enhancement of BC absorption. These results, along with the literature, indicate that MCE can provide guidance as to the general magnitude of these particle properties, but that the MCE is ultimately a fairly imprecise metric, especially for the SSA_{405nm}.

However, we find a very strong relationship between the SSA_{405nm} and the total [OA]/[BC] ratio (**Figure 1**e). This is consistent with the findings of Pokhrel et al. (2016), who observed something similar but over a smaller range of [OA]/[BC]. (Similarly strong relationships are observed for SSA values at 532 nm and 781 nm (**Figure S1**), or if the [NR-PM_1]/[BC] are used as OA averages 95% of the total NR-PM_1 mass.) Smaller [OA]/[BC] correspond to smaller SSA_{405nm} values with a sigmoidal relationship observed. (Fit parameters for all fits shown are provided in **Table S1**.) There is similarly a very strong, sigmoidal relationship between the AAE and $MAC_{BC,405nm}$ and [OA]/[BC] (**Figure 1**f,g). The large increase in the $MAC_{BC,405nm}$ indicates that BrC contributes substantially to the total absorption. The contributions of coating-induced enhancements and of BrC are discussed further in Sections 3.4.1 and 3.4.2. The larger range of [OA]/[BC] and the greater number of individual burns considered here, compared to Pokhrel et al. (2016), allows for determination of more robust fits. Pokhrel et al. (2017) found that the absorption enhancement at 405 nm, determined from thermodenuder measurements, increased with [OA]/[BC] up to [OA]/[BC] ~33 (the largest value reported), consistent with our findings.

These observations demonstrate that the optical properties of the primary particles depend on the relative amount of OA versus BC. This is as expected because OA is generally more scattering,

Deleted: Figure 1

Deleted: Figure 1

Deleted: Figure 1

Deleted: Figure 1

Deleted: Figure 1

Deleted: Figure S1

Deleted: Table S1

Formatted: Font: Bold

Deleted: Figure 1

compared to BC, and light absorbing OA (aka BrC) typically exhibits a much stronger wavelength dependence than BC. Based on these relationships, we divide the individual burns into different classes (**Table 1**). We have chosen to classify particles based on the observed SSA_{405nm} values; use of [OA]/[BC] for classification yields largely similar results, given the strong relationship between the two. The dividing lines between classes are selected to yield six classes that span the entire range of SSA_{405nm} values, from 0.23 (Class 1) to 0.97 (Class 6), with approximately equal numbers of individual burns in each class (ca. 8-10). Partitioning the observations into different particle classes facilitates interpretation of the photochemical evolution of the particles, to be discussed in future work. In addition, we find that use of the Class average properties versus MCE generally provides more representative fits to the observations (visually apparent in **Figure 1**, and supported by the reduced χ^2 for the fits).

Formatted: Font: Bold

Deleted: Table 1

Deleted: Figure 1

3.2 OA composition and volatility

Variability in the bulk composition of the OA is characterized by the O:C and H:C atomic ratios and the fractional abundance (f_x) of two marker ions, m/z = 44 and m/z = 60. The f_{44} is complementary to O:C and larger values generally indicate a greater degree of oxygenation and the presence of carboxylic acids. The f_{60} is often taken as a marker ion for biomass burning, in particular a signature of levoglucosan and similar molecules (Schneider et al., 2006;Alfarra et al., 2007). The high resolution ion $C_2H_4O_2^+$ contributes to and exhibits similar behavior as f_{60}; the slope for $f_{C2H4O2+}$ against f_{60} is 0.98. While it is known that properties such as f_{60} vary in different biomass burning samples (Schneider et al., 2006) or between near-source intercepts of different ambient plumes (Garofalo et al., 2019), the specific dependence on burn conditions or overall particle composition (e.g. [OA]/[BC]) has not been systematically explored to our knowledge.

The average f_{60} = 0.022 ± 0.01 (1σ). The f_{60} values vary non-monotonically with [OA]/[BC], exhibiting a slight increase from Class 1 to Class 3 and then a decrease from Class 4 to Class 6 (Figure 2a). This indicates that, while f_{60} is overall a useful marker ion for biomass burning, it cannot be used to distinguish between different burn conditions. The f_{44} generally decreases with [OA]/[BC] (Figure 2b; r^2 = 0.33.) However, the average f_{44} values for particle Classes 2-5 differ negligibly, suggesting that f_{44} might be useful in discriminating between extreme cases (e.g. Class 1 versus Class 6), but that it is of limited general use in distinguishing between burn conditions and fuel types. The O:C atomic ratio (average = 0.37 ± 0.09) exhibits similar behavior—expected as f_{44} is generally related to O:C (Aiken et al., 2008)—with a general decrease as [OA]/[BC] increases, although a comparably weaker correlation (Figure 2c; r^2 = 0.17). The H:C (average = 1.76 ± 0.05) exhibits a weak, positive correlation with [OA]/[BC], although the variability is slight (Figure 2d; r^2 = 0.27).

The mass fraction of the OA that is composed of nitrated organics ($f_{ON\text{-}OA}$ = [ON]/[OA]) was determined using the HR-ToF-AMS measurements and the method of Kiendler-Scharr et al. (2016) (see the Supplemental Material for further details). The terminology nitrated organics (ON) includes contributions from both nitro and nitrate functional groups. The fraction of measured nitrate that was ON ($f_{ON\text{-}N}$ = [ON]/([ON]+[NO_3^-])) decreased with [OA]/[BC] and ranged from 0.91 (Class 1) to 0.48 (Class 6) (**Figure S2a**). The Class-specific average $f_{ON\text{-}OA}$ also decreased with [OA]/[BC], although by a much greater extent than the $f_{ON\text{-}N}$, ranging from 6.0% (Class 1) to 0.27% (Class 6) and (**Figure 2e**). There is a reasonably linear relationship between log($f_{ON\text{-}OA}$) and log([OA]/[BC]) (r^2 = 0.47). This indicates that a larger proportion of ON species and functionalities are produced when particles are, on average, more BC-rich. This does not reflect differences in fuel nitrogen content as there is no relationship between fuel N and $f_{ON\text{-}OA}$ (**Figure S2b**). Therefore, it seems that the relationship between $f_{ON\text{-}OA}$ and [OA]/[BC] is related more so to the burn conditions than the fuel N content, although as with many other properties the relationship with [OA]/[BC] is clearer than with the MCE (**Figure S2c**).

The OA volatility is characterized as the ratio between the OA concentration after thermodenuding to that without thermodenuding (the mass fraction remaining, MFR_{OA}). The MFR_{OA} decreases as [OA]/[BC] increases (**Figure 2f**), indicating that the OA at lower [OA]/[BC] is less volatile than the OA at higher values. This observation provides support for the proposal by Saleh et al. (2014) that less volatile, more absorbing species are preferentially formed under conditions where BC formation is favored, discussed further in Section 3.4.2. The relationship between MFR_{OA} and [OA]/[BC] is reasonably described by an exponential function.

3.3 BC Mixing State

As discussed above, the relative amounts of OA and BC vary greatly between fuel types and combustion conditions. However, the distribution of BC and OA between particles, and how this varies between very different burn conditions, has not been previously explored in detail to our

Formatted: Font: Bold
Deleted: Figure S2
Deleted: Figure 2
Formatted: Font: Bold
Formatted: Font: Bold
Deleted: Figure S2
Deleted: Figure S2
Formatted: Font: Bold
Formatted: Font: Bold
Deleted: Figure 2

knowledge. The bulk average fraction of OA that is internally mixed with BC versus OA that is externally mixed from BC is determined using the HR-ToF-AMS and SP-AMS measurements. The HR-ToF-AMS quantifies OA independent of mixing state, whereas the SP-AMS (as operated here) quantifies only the OA that is internally mixed with BC. The fraction of OA that is internally mixed with BC ($f_{\mathrm{OA,int}}$) is:

$$f_{OA,int} = \frac{[OA]_{SP-AMS}}{[OA]_{HR-ToF-AMS}} = \frac{[OA]_{int}}{[OA]_{tot}} \qquad (5)$$

where the subscript *int* indicates the OA that is internally mixed with BC and the subscript *tot* indicates the total OA. The $f_{\mathrm{OA,int}}$ should range from 0 to 1. Related, the SP-AMS quantified the ratio between the OA that is internally mixed with BC and the BC concentration, referred to here as $[\mathrm{OA}]_{\mathrm{int}}/[\mathrm{BC}]$. We find that $f_{\mathrm{OA,int}}$ decreases substantially as [OA]/[BC] increases, ranging from $f_{\mathrm{OA,int}} = 0.4$ for Class 1 (low SSA) particles to $f_{\mathrm{OA,int}} = 0.01$ for Class 6 (high SSA) particles (**Figure 3a**). The data are well-fit by a sigmoidal function. However, the amount of OA coating BC ($R_{\mathrm{OA\text{-}BC}} = [\mathrm{OA}]_{\mathrm{int}}/[\mathrm{BC}]$) increases with the total [OA]/[BC], also with a sigmoidal relationship (**Figure 3b**). Thus, while a smaller fraction of the total OA is internally mixed with BC for larger total [OA]/[BC] the amount of OA that coats BC increases. Most likely this behavior reflects that BC and OA are generated with different efficiencies in different parts of the combusting biomass. BC is more efficiently generated from flaming combustion while OA is more efficiently generated from smoldering combustion. These observations demonstrate that the extent to which atmospheric models can assume that all OA is internally mixed with or externally mixed from BC at the point of emission will depend on the combustion conditions.

Deleted: Figure 3

Deleted: Figure 3

3.4 Absorption enhancement and brown carbon

3.4.1 Coating-induced absorption enhancement

Non- or weakly-absorbing coatings on black carbon particles can theoretically increase the absorption by BC (Fuller et al., 1999;Bond et al., 2006), an effect which has been confirmed by laboratory experiments (Lack et al., 2009;Shiraiwa et al., 2010;Cappa et al., 2012). The extent to which coatings on BC actually enhance absorption by BC in the atmosphere remains unclear. Some studies indicate minor coating-induced enhancements while others indicate substantial enhancements (Cappa et al., 2012;Healy et al., 2015;Liu et al., 2015;Peng et al., 2016;Zhang et al., 2016;Liu et al., 2017;Cappa et al., 2019b). Understanding the nature of the coating-induced enhancement is important for quantifying the radiative impacts of BC (Jacobson, 2001;Bond et al., 2013). Further, these coating-induced absorption enhancements ($E_{abs.coat}$) complicate the determination of brown carbon (BrC) absorption and the two must be separated. Here, we examine the extent to which coatings on BC for primary biomass burning particles enhance the BC absorption. Theoretically, the magnitude of $E_{abs,coat}$ for an individual particle depends primarily on the coating thickness and secondarily on the size of the BC core (Bond et al., 2006; Fuller et al., 1999). Thus, the extent to which coatings enhance BC absorption for a given situation can be assessed through the relationship between the observed MAC_{BC} and the coating-to-core mass ratio ($R_{coat\text{-}rBC}$ = [NR-PM]$_{int}$/[BC], where *int* indicates that the coating material is internally mixed with BC). The expectation is that the MAC_{BC} increases with $R_{coat\text{-}BC}$.

However, absorption by BrC can also lead to an apparent increase in the normalized absorption with R_{BC} if the BrC abundance correlates with the total coating amount. Because BrC absorbs more strongly at shorter wavelengths, the wavelength-dependence of the MAC_{BC} to R_{BC} relationship can be used to further separate the influence of coating versus BrC absorption. The MAC_{BC} exhibits a wavelength-dependent relationship with $R_{coat\text{-}rBC}$ for fresh biomass particles (405 nm, 532 nm and 781 nm) (**Figure 4a-c**). The MAC_{BC} increases notably with $R_{coat\text{-}rBC}$ at 405 nm and to a lesser extent at 532 nm. At 781 nm the MAC_{BC} is essentially independent of $R_{coat\text{-}rBC}$ up to $R_{coat\text{-}rBC}$ values as large as 10, but does exhibit some increase at $R_{coat\text{-}rBC} > 10$. However, this is most likely a result of absorption by OA at 781 nm and not indicative of an increase in the coating-induced enhancement, discussed further below. The wavelength dependence provides clear evidence of BrC absorption at shorter wavelengths.

Deleted: Figure 4

That the MAC_{BC} at 781 nm is nearly independent of $R_{coat\text{-}rBC}$ up to such large $R_{coat\text{-}rBC}$ values indicates that there is only a minor coating-induced enhancement for the primary biomass particles, the magnitude of which is discussed below. Our observations are consistent with McMeeking et al. (2014), who also investigated the relationship between the MAC_{BC} and $R_{coat\text{-}rBC}$ for a primary biomass particles from multiple fuel types. Most likely, this lack of a substantial coating-induced enhancement results from a non-even distribution of non-BC mass across the population of BC particles (Fierce et al., 2016;Liu et al., 2017) and from the morphology of BC-containing particles not conforming to an idealized core-shell structure (Adachi et al., 2010). The influence of photochemical aging on the coating-induced enhancement will be examined in future work.

Deleted: a negligible

The relationship between MAC_{BC} and the coating amount ($R_{coat\text{-}rBC}$) can be contrasted with the relationship between MAC_{BC} and the total [OA]/[BC]. At all three wavelengths the MAC_{BC} exhibit strong, sigmoidal relationships with [OA]/[BC] (**Figure 4d-f**). That $MAC_{BC,781nm}$ exhibits such a clear relationship with [OA]/[BC] suggests that even the small apparent coating-induced enhancement, implied above from the very weak with $R_{coat\text{-}rBC}$, is largely driven by absorption by BrC rather than from the impact of coating on BC. Pokhrel et al. (2017) found that the absorption enhancement, determined from thermodenuder measurements, increased notably with [OA]/[BC] up to [OA]/[BC] ~33 at 405 nm (the largest value reported by them), but by much less at 660 nm, consistent with our findings.

The observations allow for determination of wavelength-dependent MAC_{BC} values for pure BC ($MAC_{BC,pure}$) for each wavelength by extrapolation of the MAC_{BC} versus [OA]/[BC] ratio to zero using sigmoid fits. Since the $R_{coat\text{-}rBC}$ correlates reasonably with [OA]/[BC] (**Figure 3b**), extrapolation against [OA]/[BC] to zero effectively removes both contributions from BrC and any coating-induced enhancement. The derived $MAC_{BC,pure}$ values are 11.8 $m^2\ g^{-1}$ at 405 nm, 8.8 $m^2\ g^{-1}$ at 532 nm and 5.5 $m^2\ g^{-1}$ at 781 nm, with estimated fit-based uncertainties of ~10%. The absolute uncertainties on the $MAC_{BC,pure}$ are primarily dependent on the uncertainty in the b_{abs} and [rBC] measurements, and are ~35%. The derived MAC_{BC} values are very similar to those recently reported by Forestieri et al. (2018) for fresh BC particles: $MAC_{BC,pure}$ = 11.9 $m^2\ g^{-1}$ at 405 nm and 8.8 $m^2\ g^{-1}$ at 532 nm, with an extrapolated value at 781 nm of 5.7 $m^2\ g^{-1}$. The value at 532 nm is somewhat higher than that suggested by Bond and Bergstrom (2006) (7.75 $m^2\ g^{-1}$ at 532 nm). Our derived $MAC_{BC,pure}$ values yield an AAE = 1.17, determined from a fit to the three wavelengths. An AAE close to unity indicates absorption is dominated by BC, as expected.

Values for the absorption enhancement at 781 nm are calculated as the ratio between the observed MAC_{BC} in **Figure 4** and the derived $MAC_{BC,pure}$. The derived E_{abs} range from 0.96 to 27. Values greater than two occur only for the particles having particularly large [OA]/[BC], > 400. As E_{abs} values much greater than two at 781 nm are unlikely to result from mixing-induced enhancements (Chakrabarty and Heinson, 2018), this again suggests that the OA is somewhat absorbing at this wavelength. For the burns where [OA]/[BC] < 400, the median E_{abs} = 1.14 and the arithmetic mean E_{abs} = 1.19 ± 0.14 (1σ). Given that some of this enhancement may result from BrC absorption at 781, these values can be considered upper-limits on $E_{abs,coat}$, and the small

Deleted: Figure 4

Deleted: r

Deleted: Figure 3

Formatted: Font: Symbol

magnitude is consistent with our conclusion above that, while likely greater than zero, the mixing-induced enhancement is generally negligible. It is possible that the $E_{abs,coat}$ values when [OA]/[BC] > 400 are substantially larger. However, given the general lack of a dependence of the $MAC_{BC,781nm}$ for $R_{BC\text{-}coat}$ < 10 this seems unlikely.

3.4.2 Primary brown carbon absorption

The absorption due to brown carbon is determined by difference as:

$$\boldsymbol{b_{abs,BrC} = b_{abs,obs} - MAC_{BC,pure} \cdot [BC] \cdot E_{abs,coat}} \qquad \textbf{(6)}$$

where $b_{abs,BrC}$ is the absorption due to BrC specifically. Importantly, the use of study-specific $MAC_{BC,pure}$ values serves to reduce systematic biases in the $b_{abs,BrC}$, compared to direct use of literature $MAC_{BC,pure}$ values. Assuming $E_{abs,coat}$ = 1 provides an upper limit on the BrC absorption, which we note is likely most appropriate for the particles sampled here, as discussed in the previous section. Therefore, we use the upper-limit values throughout the analysis that follows, unless otherwise stated. However, a lower limit for BrC absorption can be determined at 405 nm and 532 nm assuming that all of the enhancement at 781 nm results from coatings and not from BrC. The resulting $E_{abs,obs}$ (= $MAC_{BC,obs}/MAC_{BC,pure}$) at 781 nm averages 1.19 for $R_{BC\text{-}coat}$ < 10. Using $E_{abs,coat}$ = 1.19 in Eqn. 7 yields a lower limit for the BrC absorption at the two shorter wavelengths, appropriate since $E_{abs,coat}$ generally has only a small wavelength dependence. A fit to the coating-corrected (lower-limit) versus upper-limit $b_{abs,BrC}$ yields a slope of 0.97 at 405 nm and 0.88 at 532 nm (**Figure S3**). The smaller difference at 405 nm results from the fractional contribution of BrC to the total absorption being larger at this wavelength.

Brown carbon-specific mass absorption coefficients (MAC_{BrC}) are determined as the ratio between $b_{abs,BrC}$ and the total OA concentration:

$$\boldsymbol{MAC_{BrC} = \frac{b_{abs,BrC}}{[OA]}} \qquad (7)$$

The MAC_{BrC} values from Eqn. **7** are bulk-average values, and do not account for different molecules and classes of molecules likely having different absorptivities. Uncertainties in the MAC_{BrC} values are determined by error propagation. Similarly, an AAE value for just the brown carbon (AAE_{BrC}) can be calculated using wavelength pairs as:

Deleted: Figure S3

$$\boldsymbol{AAE_{BrC}} = -\log\left(\frac{b_{abs,BrC,\lambda_1}}{b_{abs,BrC,\lambda_2}}\right) / \log\left(\frac{\lambda_1}{\lambda_2}\right); \tag{8}$$

The geometric averages of the *MAC*$_{BrC}$ values are $0.76^{+0.65}_{-0.35}$ m^2 g^{-1}, $0.21^{+0.36}_{-0.13}$ m^2 g^{-1}, $0.056^{+0.15}_{-0.04}$ m^2 g^{-1} at 405 nm, 532 nm and 781 nm, with uncertainties the 1σ burn-to-burn variability. The *MAC*$_{BrC}$ values vary between classes, generally increasing as the [OA]/[BC] ratio decreases at all wavelengths (shown for 405 nm in **Figure 5**a). For example, the average *MAC*$_{405nm}$ = 2.3 ± 1 m^2 g^{-1} for Class 1 and 0.35 ± 0.09 m^2 g^{-1} for Class 6. Although the uncertainties on the derived *MAC*$_{BrC}$ increase substantially as [OA]/[BC] decreases—because BrC absorption contributes to a smaller extent at longer wavelengths—the observations nonetheless indicate that the BrC absorptivity depends on the combustion conditions. The relationship at 405 nm is well-described by a sigmoidal function in log-log space, with limiting values of 0.35 m^2 g^{-1} at large [OA]/[BC] and 11.2 m^2 g^{-1} at small [OA]/[BC]. That the extrapolated zero [OA]/[BC] limit for *MAC*$_{BrC}$ is similar to pure BC suggests an evolution of BrC towards having properties similar to BC when the overall [OA] content is small. Such behavior is consistent with Saleh et al. (2018), who argue that there is a continuum of BrC properties that depends on the combustion conditions, as demonstrated in that study for low-temperature benzene and toluene combustion. The range of the *MAC*$_{BrC}$ values observed here, including that there is notable absorption at 781 nm, encompass many previous measurements, summarized in **Table S3**. This likely reflects the wide diversity of fuel types and burn conditions considered here, as exemplified by the very large range of [OA]/[BC].

Estimated values of the imaginary component of the refractive index for BrC (k_{BrC}) are determined from Mie theory via optical closure (Zhang et al., 2016), assuming a real part of the refractive index of 1.5 and a particle diameter of 150 nm, a typical value for these experiments. Imaginary RI values are of use in atmospheric models for calculation of BrC absorption. There is a linear relationship between *MAC*$_{BrC}$ and k_{BrC} (**Figure S4**a). Thus, the k_{BrC} exhibits a similar correlation with [OA]/[BC] as does the *MAC*$_{BrC}$ (**Figure 5**a).

The wavelength-dependence of absorption, i.e. the *AAE*$_{405\text{-}532}$, also varies with [OA]/[BC], in this case with a positive relationship between the two (**Figure 5**b). The relationship is reasonably described by a sigmoidal function. This implies that, while the *MAC*$_{BrC}$ varies inversely with [OA]/[BC] at all wavelengths, the exact variation is wavelength dependent. The *AAE*$_{405\text{-}532}$ relationship with [OA]/[BC] is well-described by a sigmoidal function (versus log([OA]/[BC]),

Deleted: Figure 5

Deleted: observed

Deleted: values

Formatted: Font: Bold

Deleted: Table S3

Deleted: Figure S4

Deleted: Figure 5

Deleted: Figure 5

with limiting values of 10.4 at large [OA]/[BC] and 1.3 at small [OA]/[BC]. The wavelength-dependence of the k_{BrC} (w_{BrC}) are also calculated, to facilitate comparison with the literature, as:

$$w_{BrC} = -\log\left(\frac{k_{BrC,\lambda 1}}{k_{BrC,\lambda 2}}\right)/\log\left(\frac{\lambda 1}{\lambda 2}\right) \quad (9)$$

The w_{BrC} exhibit a similar dependence on [OA]/[BC] as the AAE_{BrC}, as the w_{BrC} and AAE_{BrC} are linearly related, albeit with some scatter (**Figure S4**b; $r^2 = 0.97$).

Deleted: Figure S4

Our observations support the results of Saleh et al. (2014), who also found a relationship between the $k_{BrC,405nm}$ and [OA]/[BC]. However, our analysis substantially extends the range of [OA]/[BC] values investigated in that work (they considered [OA]/[BC] from only ca. 2 to 170). In the overlap region between our two studies the $k_{BrC,405nm}$ agree reasonably well over the range 2 < [OA]/[BC] < 50, but the $k_{BrC,405nm}$ from Saleh et al. (2014) are smaller than observed here above [OA]/[BC] = 50. Importantly, our results demonstrate that the linear fit suggested by Saleh et al. (2014) for MAC_{BrC} is only appropriate over the range of values they considered and that a sigmoidal provides for a more robust relationship over a wider range of [OA]/[BC]. Related, the wider range of [OA]/[BC] enables more robust determination of the functional dependence of the wavelength-dependence of absorption (w_{BrC}), with overall larger w_{BrC} values and a larger plateau at high [OA]/[BC] compared to the fit by Saleh et al. (2014).

The MAC_{BrC} values also correlate with the nitrated organic fraction of OA, the latter of which, as noted above, also correlates with the [OA]/[BC] (**Figure 6**a). This observation suggests that organic nitrate and nitro functionalities may be at least somewhat responsible for the increase in absorption. Laskin et al. (2018) performed offline molecular level analyses of primary OA collected during FIREX. They found that nitroaromatics and N-containing polycyclic aromatic hydrocarbons (PAHs) contribute notably to the total light absorption by BrC, although there are many non-N-containing species that also contribute to BrC absorption. The variability between particle Classes is consistent with the results of Lin et al. (2016), which show that the abundance of N-containing chromophores varies between particles produced from different biomass fuels. Additionally Mohr et al. (2013) observed a relationship between the concentration of nitrated phenols and short-wavelength absorption by BrC, although it is possible that for their measurements these species were produced from chemical processing, as opposed to being directly emitted. Altogether, our results provide support for the idea that nitrated organic functionalities

Deleted: Figure 6

are an important contributor to BrC absorption. However, it is very likely that other functional groups also contribute to the total absorption.

The $MAC_{\mathrm{BrC,405nm}}$ exhibits an inverse correlation with the f_{60}/f_{44} ratio of the OA, although there is substantial scatter in the f_{60}/f_{44} ratio for a given particle class (**Figure 6**b). (The f_{44} and f_{60} have no discernable relationship.) The observed $MAC_{\mathrm{BrC,405nm}}$ relationship with f_{60}/f_{44} is opposite that reported by Lack et al. (2013) for ambient measurements of particles a biomass burning plume, who find a reasonable positive correlation. This difference in behavior results from our sampling primary particles directly—thereby focusing on the inherent variability in the properties of the emitted particles—while Lack et al. (2013) sampled ambient particles. For ambient sampling, the observed relationship will be sensitive to mixing of biomass burning particles with background or aged biomass particles, which are known to have a smaller f_{60} (Cubison et al., 2011). Thus, the relationship observed by Lack et al. (2013) can best be viewed as a mixing line between the fresh primary particles (having large $MAC_{\mathrm{BrC,405nm}}$ and large f_{60}/f_{44}) and background or aged biomass particles (having small $MAC_{\mathrm{BrC,405nm}}$ and small f_{60}/f_{44}), rather than providing information on the inherent variability in the absorptivity of the fresh particles.

Deleted: Figure 6

3.5 Size distributions

Total particle mobility size distributions and BC-only size distributions were measured (**Figure 7**). Primary particle size distributions are important parameters specified in regional and global models. The number-weighted and volume-weighted size distributionare generally described by either one or two log-normal modes for individual burns; a two-mode fit provides a more robust solution across all modes. The mass-weighted BC size distributions are similarly described by one or two log-normal modes. A fit to the average number-weighted distribution across all particle classes yields geometric median diameters ($d_{p,N}$) and widths (σ_g) of 60.3 nm and 1.76, respectively, for the smaller mode and 153 nm and 1.64 for the larger mode (**Figure 8**). The amplitude of the smaller mode is 4.6 times the larger mode. A single mode fit yields $d_{p,N}$ = 68 nm and χ_g = 1.93, although the fit is poorer. Mann et al. (2014) report $d_{p,N}$ values used by a variety of global models for biofuels. The models tend to use either 80 nm or 150 nm, although a few use other values (30 nm, 60 nm, 100 nm). Those using 80 nm typically use σ_g = 1.80 while those using 150 nm typically use σ_g = 1.59, although there are exceptions. Our observations indicate that use of a bimodal

Deleted: Figure 7

Deleted: Figure 8

distribution within models would be more representative, but that a single mode can do acceptably. We find that the volume-weighted distribution calculated from a single-mode fit to the number-weighted distribution is similar to the observed volume-weighted distribution (**Figure 8**). Thus, the use of a single-mode to represent biomass burning size distributions thus appears acceptable, so long as the appropriate parameters are used. In this context, the widths of the distribution used by the various global models appear somewhat too small. However, we note that the microphysics occurring in the fresh smoke sampled here, which will govern the size distributions, may differ from that in atmospheric plumes.

Deleted: Figure 8

The average BC-specific mass-weighted size distribution mode is at 148 nm (**Figure 8**). A bimodal fit yields values for the mass median diameter ($d_{p,M}$) and σ_g of 137.2 nm and 1.62, respectively, for the smaller mode and 197.1 nm and 1.24 for the larger mode, with most of the mass contained in the smaller mode. May et al. (2014) report $d_{p,M}$ from laboratory biomass combustion ranging from 140-190 nm, averaging 170 nm. Their average is somewhat larger than ours, likely reflecting differences in the exact fuels sampled. The mode diameter for the BC-specific distribution is especially smaller than observed for biomass burning particles from some ambient observations, which tend to give values closer to 200 nm (Schwarz et al., 2008;Kondo et al., 2011;Sahu et al., 2012;May et al., 2014;Cappa et al., 2019b). This difference between lab and field observations was also noted by May et al. (2014). We speculate that the influence of coagulation may be suppressed in our experiments relative to what occurs in the atmosphere due to slower overall dilution, leading to smaller BC size distributions. To the extent this is the reason for the difference, the total particle distributions would also be biased towards too small particles, compared to the atmosphere. However, there is no relationship between $d_{p,N}$ and the total particle number concentration for our experiments. Formation of secondary aerosol in the near-field of a sampled ambient plume could also contribute to this difference.

Deleted: Figure 8

There is substantial variability between individual burns within a given particle Class in terms of the shape of the size distributions (**Figure 7**). This variability is most evident for Class 1, 2 and 5, but present for all Classes. Nonetheless, the number-weighted mean diameter ($d_{p,N,mean}$) appears to decrease somewhat with MCE (**Figure 9**; $r^2 = 0.38$). However, the relationship is largely driven by the Class 6 particles, which generally have lower MCE values, having larger $d_{p,N,mean}$ values. A lack of any particularly clear relationship is consistent with Hosseini et al. (2010), who observed

Deleted: Figure 7

Deleted: Figure 9

the $d_{p,N,mean}$ to exhibit a complex relationship with combustion conditions. The $d_{p,N,mean}$ varies non-monotonically with [OA]/[BC], with particle size first decreasing slightly as [OA]/[BC] increases (from Class 1 to Class 3) and then increasing with further increases in [OA]/[BC] (from Class 4 to Class 6) (Figure 9). This is despite the notable burn-to-burn variability. It is important to note that the mobility-based size is particle shape-dependent; very BC-rich particles are more likely to have non-spherical shapes and thus have larger mobility diameters. This could explain the minimum in $d_{p,N}$ around Class 3 particles, for which [OA]/[BC] = 10.

Some of the variability within a class appears related to the presence of different fuel types within a class. Number-weighted and BC-specific mass-weighted size distributions by fuel type are shown in Figure 10. For the number-weighted distributions, leaf litter and rotten logs exhibit the greatest variability between different burns, although we note that multiple burns were not performed for all fuels. The shapes of the leaf litter, peat and "other" fuel types differ most notably from the other fuel types, with the presence of more than one mode more apparent. (The "other" category here includes non-traditional biofuels, specifically building materials and excelsior.) For the BC-specific size distributions, the litter, canopy, and duff exhibited the greatest intra-fuel variability. For most fuels, the BC-specific distribution peaks around 150 nm, as noted above. However, for a subset of burns (eight of them) the BC-specific distribution peaks around 100 nm (Figure 10). These small BC-mode distributions occur for the OA-rich particle classes 4, 5 and 6 (Figure 7), although there is no clear pattern to their occurrence.

Deleted: Figure 9

Deleted: Figure 10

Deleted: Figure 10

Deleted: Figure 7

4 Conclusions and Implications

Measurements of primary particles produced from combustion of a variety of biomass fuel types indicate the optical, physical, and chemical properties of the emitted particles exhibit wide variability. We show that variability in many optical properties (e.g. single scatter albedo, wavelength dependence of absorption, mass absorptivity of black and brown carbon) is directly linked to the [OA]/[BC] ratio of the emitted particles; the relationships with [OA]/[BC] are much stronger than with the commonly used modified combustion efficiency, and mathematical relationships between the various properties are determined. However, the absorption enhancement due to coating of BC (the so-called "lensing" effect) is shown to be negligible and essentially independent of the amount of coating up to large coating-to-BC mass ratios. The brown carbon mass absorptivity correlates with the nitrated organic fraction of OA, suggesting that nitrated organic species contribute to BrC absorption. Many bulk chemical properties (i.e. O:C, H:C, and the relative concentrations of key marker ions such as f_{60}) exhibit limited dependence on the burn conditions and the [OA]/[BC] ratio. However, both the OA volatility and nitrated organic fraction of OA decrease with [OA]/[BC]. The fraction of OA that is internally mixed with BC was shown to decrease strongly with the [OA]/[BC] ratio, from nearly all OA being internally mixed with BC when the particles are overall BC-rich to only a few percent of OA being mixed with BC when OA dominates. Yet, the relative amount of OA coating the BC increases with [OA]/[BC]; that is, when more of the OA is externally mixed from BC those particles that do contain BC nonetheless have thicker OA coatings. The observed total particle size distributions are reasonably well described by a single log-normal mode, but are better fit using a bimodal distribution. The BC-specific size distributions are similarly best fit using a bimodal distribution, although a single mode provides a reasonable representation. The dependence of the geometric median mobility diameter on the burn conditions or particle state (i.e. the [OA]/[BC]) is complicated by the mobility diameter being sensitive to variations in particle shape, which depend on the [OA]/[BC] ratio. Overall, these results expand on previous observations of primary biomass burning particle properties, considering a wider range of [OA]/[BC] and associated properties. Further, they provide a foundation for understanding the post-emission evolution of biomass burning smoke due to photochemical oxidation as discussed in Lim et al. (2019).

5 Data Availability

All data are available from the NOAA FIREX-AQ data repository (https://esrl.noaa.gov/csd/projects/firex/firelab/). This includes a summary of the fuel types used for each burn and the measurement time-series for each burn. The primary particle averages used in this work are additionally collected in the UC DASH data repository (Cappa et al., 2019a).

6 Author Contributions

CDC and JHK designed the experiments. CDC, CYL, and DHH carried out the measurements and data processing. CDC, CDM, and CYL analyzed data. CDC and CDM wrote the manuscript, with contributions from all co-authors.

7 Acknowledgements

This work was supported by the National Oceanic and Atmospheric Administration Atmospheric Chemistry, Carbon Cycle & Climate Program, awards NA16OAR4310111 and NA16OAR4310112. CYL was additionally supported by the National Science Foundation Graduate Research Fellowship Program. The entire FIREX team, especially Bob Yokelson and Jim Roberts and the staff of the Missoula Fire Sciences Laboratory, are acknowledged for their assistance. Putting together the community inlet was a community effort—thank you to all who contributed. Shuka Schwarz and Gavin McMeeking are also thanked for their assistance with the SP2.

8 References

Adachi, K., Chung, S. H., and Buseck, P. R.: Shapes of soot aerosol particles and implications for their effects on climate, J. Geophys. Res., 115, D15206, https://doi.org/10.1029/2009jd012868, 2010.

Adler, G., Flores, J. M., Abo Riziq, A., Borrmann, S., and Rudich, Y.: Chemical, physical, and optical evolution of biomass burning aerosols: a case study, Atmos. Chem. Phys., 11, 1491-1503, https://doi.org/10.5194/acp-11-1491-2011, 2011.

Aiken, A. C., Decarlo, P. F., Kroll, J. H., Worsnop, D. R., Huffman, J. A., Docherty, K. S., Ulbrich, I. M., Mohr, C., Kimmel, J. R., Sueper, D., Sun, Y., Zhang, Q., Trimborn, A., Northway, M., Ziemann, P. J., Canagaratna, M. R., Onasch, T. B., Alfarra, M. R., Prevot, A. S. H., Dommen, J., Duplissy, J., Metzger, A., Baltensperger, U., and Jimenez, J. L.: O/C and OM/OC ratios of primary, secondary, and ambient organic aerosols with high-resolution time-of-flight aerosol mass spectrometry, Environ. Sci. Technol., 42, 4478-4485, https://doi.org/10.1021/es703009q, 2008.

Alexander, D. T. L., Crozier, P. A., and Anderson, J. R.: Brown Carbon Spheres in East Asian Outflow and Their Optical Properties, Science, 321, 833-836, https://doi.org/10.1126/science.1155296, 2008.

Alfarra, M. R., Prevot, A. S. H., Szidat, S., Sandradewi, J., Weimer, S., Lanz, V. A., Schreiber, D., Mohr, M., and Baltensperger, U.: Identification of the Mass Spectral Signature of Organic Aerosols from Wood Burning Emissions, Environmental Science & Technology, 41, 5770-5777, https://doi.org/10.1021/es062289b, 2007.

Andreae, M. O., and Merlet, P.: Emission of trace gases and aerosols from biomass burning, Global Biogeochemical Cycles, 15, 955-966, https://doi.org/doi:10.1029/2000GB001382, 2001.

Bluvshtein, N., Lin, P., Flores, J. M., Segev, L., Mazar, Y., Tas, E., Snider, G., Weagle, C., Brown, S. S., Laskin, A., and Rudich, Y.: Broadband optical properties of biomass-burning aerosol and identification of brown carbon chromophores, Journal of Geophysical Research: Atmospheres, 122, 5441-5456, https://doi.org/doi:10.1002/2016JD026230, 2017.

Bond, T. C., and Bergstrom, R. W.: Light absorption by carbonaceous particles: An investigative review, Aerosol Science and Technology, 40, 27-67, https://doi.org/10.1080/02786820500421521, 2006.

Bond, T. C., Habib, G., and Bergstrom, R. W.: Limitations in the enhancement of visible light absorption due to mixing state, J. Geophys. Res.-Atmos., 111, https://doi.org/10.1029/2006JD007315, 2006.

Bond, T. C., Doherty, S. J., Fahey, D. W., Forster, P. M., Berntsen, T., DeAngelo, B. J., Flanner, M. G., Ghan, S., Kärcher, B., Koch, D., Kinne, S., Kondo, Y., Quinn, P. K., Sarofim, M. C., Schultz, M. G., Schulz, M., Venkataraman, C., Zhang, H., Zhang, S., Bellouin, N., Guttikunda, S. K., Hopke, P. K., Jacobson, M. Z., Kaiser, J. W., Klimont, Z., Lohmann, U., Schwarz, J. P., Shindell, D., Storelvmo, T., Warren, S. G., and Zender, C. S.: Bounding the role of black carbon in the climate system: A scientific assessment, Journal of Geophysical Research: Atmospheres, 118, 1-173, https://doi.org/10.1002/jgrd.50171, 2013.

Bruns, E. A., Perraud, V., Zelenyuk, A., Ezell, M. J., Johnson, S. N., Yu, Y., Imre, D., Finlayson-Pitts, B. J., and Alexander, M. L.: Comparison of FTIR and Particle Mass Spectrometry for the

Measurement of Particulate Organic Nitrates, Environmental Science & Technology, 44, 1056-1061, https://doi.org/10.1021/es9029864, 2010.

Canagaratna, M. R., Jayne, J. T., Jimenez, J. L., Allan, J. D., Alfarra, M. R., Zhang, Q., Onasch, T. B., Drewnick, F., Coe, H., Middlebrook, A., Delia, A., Williams, L. R., Trimborn, A. M., Northway, M. J., DeCarlo, P. F., Kolb, C. E., Davidovits, P., and Worsnop, D. R.: Chemical and microphysical characterization of ambient aerosols with the Aerodyne aerosol mass spectrometer, Mass Spectrometry Reviews, 26, 185-222, https://doi.org/10.1002/mas.20115, 2007.

Cappa, C. D., Onasch, T. B., Massoli, P., Worsnop, D., Bates, T. S., Cross, E., Davidovits, P., Hakala, J., Hayden, K., Jobson, B. T., Kolesar, K. R., Lack, D. A., Lerner, B., Li, S. M., Mellon, D., Nuaanman, I., Olfert, J., Petaja, T., Quinn, P. K., Song, C., Subramanian, R., Williams, E. J., and Zaveri, R. A.: Radiative absorption enhancements due to the mixing state of atmospheric black carbon, Science, 337, 1078-1081, https://doi.org/10.1126/science.1223447, 2012.

Cappa, C. D., Lim, C. Y., Hagan, D. H., and Kroll, J. H.: Measurements from the Fire Influence on Regional and Global Environments Experiment (FIREX) Fire Lab Mini Chamber Experiment, UC Davis DASH, Dataset, version 1, https://doi.org/10.25338/B8CK5N, 2019a.

Cappa, C. D., Zhang, X., Russell, L. M., Collier, S., Lee, A. K. Y., Chen, C.-L., Betha, R., Chen, S., Liu, J., Price, D. J., Sanchez, K. J., McMeeking, G., Williams, L. R., Onasch, T. B., Worsnop, D. R., Abbatt, J., and Zhang, Q.: Light absorption by ambient black and brown carbon and its dependence on black carbon coating state for two California, USA cities in winter and summer, Journal of Geophysical Research-Atmospheres, https://doi.org/10.1029/2018JD029501, 2019b.

Chakrabarty, R. K., Moosmüller, H., Chen, L. W. A., Lewis, K., Arnott, W. P., Mazzoleni, C., Dubey, M. K., Wold, C. E., Hao, W. M., and Kreidenweis, S. M.: Brown carbon in tar balls from smoldering biomass combustion, Atmospheric Chemistry and Physics, 10, 6363-6370, https://doi.org/10.5194/acp-10-6363-2010, 2010.

Chakrabarty, R. K., and Heinson, W. R.: Scaling Laws for Light Absorption Enhancement Due to Nonrefractory Coating of Atmospheric Black Carbon Aerosol, Physical Review Letters, 121, 218701, https://doi.org/10.1103/PhysRevLett.121.218701, 2018.

Chen, Y., and Bond, T. C.: Light absorption by organic carbon from wood combustion, Atmos. Chem. Phys., 10, 1773-1787, https://doi.org/10.5194/acp-10-1773-2010, 2010.

Coggon, M. M., Lim, C. Y., Koss, A. R., Sekimoto, K., Yuan, B., Cappa, C. D., Kroll, J. H., Selimovic, V., Zarzana, K. J., Brown, S. S., Roberts, J. M., Müller, M., Yokelson, R. J., Wisthaler, A., Krechmer, J., Jimenez, J. L., De Gouw, J., and Warneke, C.: OH-chemistry of volatile organic compounds emitted from laboratory and ambient biomass burning smoke: Influence of furans and oxygenated aromatics on ozone and secondary VOC formation., Atmos. Chem. Phys. Discuss., https://doi.org/10.5194/acp-2019-516, 2019.

Collier, S., Williams, L. R., Onasch, T. B., Cappa, C. D., Zhang, X., Russell, L. M., Chen, C.-L., Sanchez, K. J., Worsnop, D. R., and Zhang, Q.: Influence of emissions and aqueous processing on particles containing black carbon in a polluted urban environment: Insights from a soot particle – aerosol mass spectrometer, Journal of Geophysical Research-Atmospheres, *123*, 6648-6666, https://doi.org/10.1002/2017JD027851, 2018.

Cubison, M. J., Ortega, A. M., Hayes, P. L., Farmer, D. K., Day, D., Lechner, M. J., Brune, W. H., Apel, E., Diskin, G. S., Fisher, J. A., Fuelberg, H. E., Hecobian, A., Knapp, D. J., Mikoviny, T., Riemer, D., Sachse, G. W., Sessions, W., Weber, R. J., Weinheimer, A. J., Wisthaler, A., and Jimenez, J. L.: Effects of aging on organic aerosol from open biomass burning smoke in aircraft and laboratory studies, Atmos. Chem. Phys., 11, 12049-12064, https://doi.org/10.5194/acp-11-12049-2011, 2011.

Fierce, L., Bond, T. C., Bauer, S. E., Mena, F., and Riemer, N.: Black carbon absorption at the global scale is affected by particle-scale diversity in composition, Nat. Comm., 7, https://doi.org/10.1038/ncomms12361, 2016.

Forestieri, S. D., Helgestad, T. M., Lambe, A. T., Renbaum-Wolff, L. H., Lack, D. A., Massoli, P., Cross, E. S., Dubey, M. K., Mazzoleni, C., Olfert, J., Freedman, A., Davidovits, P., Onasch, T. B., and Cappa, C. D.: Measurement and modeling of the multi-wavelength optical properties of uncoated flame-generated soot, Atmos. Chem. Phys., 18, 12141-12159, https://doi.org/10.5194/acp-18-12141-2018, 2018.

Forrister, H., Liu, J., Scheuer, E., Dibb, J., Ziemba, L., Thornhill, K. L., Anderson, B., Diskin, G., Perring, A. E., Schwarz, J. P., Campuzano-Jost, P., Day, D. A., Palm, B. B., Jimenez, J. L., Nenes, A., and Weber, R. J.: Evolution of brown carbon in wildfire plumes, Geophysical Research Letters, 42, 4623-4630, https://doi.org/10.1002/2015GL063897, 2015.

Fuller, K. A., Malm, W. C., and Kreidenweis, S. M.: Effects of mixing on extinction by carbonaceous particles, J. Geophys. Res.-Atmos., 104, 15941-15954, https://doi.org/10.1029/1998jd100069, 1999.

Garofalo, L. A., Pothier, M. A., Levin, E. J. T., Campos, T., Kreidenweis, S. M., and Farmer, D. K.: Emission and Evolution of Submicron Organic Aerosol in Smoke from Wildfires in the Western United States, ACS Earth and Space Chem., 3, 1237-1247, https://doi.org/10.1021/acsearthspacechem.9b00125, 2019.

Healy, R., Wang, J., Jeong, C. H., Lee, A., Willis, M., Jaroudi, E., Zimmerman, N., Hilker, N., Murphy, M., and Eckhardt, S.: Light-absorbing properties of ambient black carbon and brown carbon from fossil fuel and biomass burning sources, Journal of Geophysical Research: Atmospheres, 120, 6619-6633, 2015.

Hoffer, A., Gelencser, A., Guyon, P., Kiss, G., Schmid, O., Frank, G. P., Artaxo, P., and Andreae, M. O.: Optical properties of humic-like substances (HULIS) in biomass-burning aerosols, Atmospheric Chemistry and Physics, 6, 3563-3570, 2006.

Hoffer, A., Tóth, A., Nyirő-Kósa, I., Pósfai, M., and Gelencsér, A.: Light absorption properties of laboratory-generated tar ball particles, Atmos. Chem. Phys., 16, 239-246, https://doi.org/10.5194/acp-16-239-2016, 2016.

Hosseini, S., Li, Q., Cocker, D., Weise, D., Miller, A., Shrivastava, M., Miller, J. W., Mahalingam, S., Princevac, M., and Jung, H.: Particle size distributions from laboratory-scale biomass fires using fast response instruments, Atmos. Chem. Phys., 10, 8065-8076, https://doi.org/10.5194/acp-10-8065-2010, 2010.

Jacobson, M. Z.: Strong radiative heating due to the mixing state of black carbon in atmospheric aerosols, Nature, 409, 695-697, https://doi.org/10.1038/35055518, 2001.

Jen, C. N., Hatch, L. E., Selimovic, V., Yokelson, R. J., Weber, R., Fernandez, A. E., Kreisberg, N. M., Barsanti, K. C., and Goldstein, A. H.: Speciated and total emission factors of particulate organics from burning western U.S. wildland fuels and their dependence on combustion efficiency, Atmos. Chem. Phys., 19, 1013-1026, https://doi.org/10.5194/acp-19-1013-2019, 2019.

Kiendler-Scharr, A., Mensah, A. A., Friese, E., Topping, D., Nemitz, E., Prevot, A. S. H., Äijälä, M., Allan, J., Canonaco, F., Canagaratna, M., Carbone, S., Crippa, M., Dall Osto, M., Day, D. A., De Carlo, P., Di Marco, C. F., Elbern, H., Eriksson, A., Freney, E., Hao, L., Herrmann, H., Hildebrandt, L., Hillamo, R., Jimenez, J. L., Laaksonen, A., McFiggans, G., Mohr, C., O'Dowd, C., Otjes, R., Ovadnevaite, J., Pandis, S. N., Poulain, L., Schlag, P., Sellegri, K., Swietlicki, E., Tiitta, P., Vermeulen, A., Wahner, A., Worsnop, D., and Wu, H.-C.: Ubiquity of organic nitrates from nighttime chemistry in the European submicron aerosol, Geophysical Research Letters, 43, 7735-7744, https://doi.org/doi:10.1002/2016GL069239, 2016.

Kirchstetter, T. W., Novakov, T., and Hobbs, P. V.: Evidence that the spectral dependence of light absorption by aerosols is affected by organic carbon, Journal of Geophysical Research-Atmospheres, 109, D21208, 2004.

Kondo, Y., Matsui, H., Moteki, N., Sahu, L., Takegawa, N., Kajino, M., Zhao, Y., Cubison, M. J., Jimenez, J. L., Vay, S., Diskin, G. S., Anderson, B., Wisthaler, A., Mikoviny, T., Fuelberg, H. E., Blake, D. R., Huey, G., Weinheimer, A. J., Knapp, D. J., and Brune, W. H.: Emissions of black carbon, organic, and inorganic aerosols from biomass burning in North America and Asia in 2008, J. Geophys. Res., 116, D08204, https://doi.org/10.1029/2010jd015152, 2011.

Koss, A. R., Sekimoto, K., Gilman, J. B., Selimovic, V., Coggon, M. M., Zarzana, K. J., Yuan, B., Lerner, B. M., Brown, S. S., Jimenez, J. L., Krechmer, J., Roberts, J. M., Warneke, C., Yokelson, R. J., and de Gouw, J.: Non-methane organic gas emissions from biomass burning: identification, quantification, and emission factors from PTR-ToF during the FIREX 2016 laboratory experiment, Atmos. Chem. Phys., 18, 3299-3319, https://doi.org/10.5194/acp-18-3299-2018, 2018.

Lack, D. A., Cappa, C. D., Cross, E. S., Massoli, P., Ahern, A. T., Davidovits, P., and Onasch, T. B.: Absorption Enhancement of Coated Absorbing Aerosols: Validation of the Photo-Acoustic Technique for Measuring the Enhancement, Aerosol Science and Technology, 43, 1006-1012, https://doi.org/10.1080/02786820903117932, 2009.

Lack, D. A., Langridge, J., Bahreni, R., Cappa, C. D., Middlebrook, A., and Schwarz, J. P.: Brown Carbon and Internal Mixing in Biomass Burning Particles, PNAS, 10, 14802-14807, https://doi.org/10.1073/pnas.1206575109, 2012a.

Lack, D. A., Richardson, M. S., Law, D., Langridge, J. M., Cappa, C. D., McLaughlin, R. J., and Murphy, D. M.: Aircraft Instrument for Comprehensive Characterization of Aerosol Optical Properties, Part 2: Black and Brown Carbon Absorption and Absorption Enhancement Measured with Photo Acoustic Spectroscopy, Aerosol Science and Technology, 46, 555-568, https://doi.org/10.1080/02786826.2011.645955, 2012b.

Lack, D. A., Bahreini, R., Langridge, J. M., Gilman, J. B., and Middlebrook, A. M.: Brown carbon absorption linked to organic mass tracers in biomass burning particles, Atmos. Chem. Phys., 13, 2415-2422, https://doi.org/10.5194/acp-13-2415-2013, 2013.

Langridge, J. M., Richardson, M. S., Lack, D., Law, D., and Murphy, D. M.: Aircraft Instrument for Comprehensive Characterization of Aerosol Optical Properties, Part I: Wavelength-Dependent Optical Extinction and Its Relative Humidity Dependence Measured Using Cavity Ringdown Spectroscopy, Aerosol Science and Technology, 45, 1305-1318, https://doi.org/10.1080/02786826.2011.592745, 2011.

Laskin, A., Lin, P., Laskin, J., Fleming, L. T., and Nizkorodov, S.: Molecular Characterization of Atmospheric Brown Carbon, in: Multiphase Environmental Chemistry in the Atmosphere, ACS Symposium Series, 1299, American Chemical Society, 261-274, 2018.

Levin, E. J. T., McMeeking, G. R., Carrico, C. M., Mack, L. E., Kreidenweis, S. M., Wold, C. E., Moosmüller, H., Arnott, W. P., Hao, W. M., Collett, J. L., and Malm, W. C.: Biomass burning smoke aerosol properties measured during Fire Laboratory at Missoula Experiments (FLAME), Journal of Geophysical Research: Atmospheres, 115, D18210, https://doi.org/10.1029/2009JD013601, 2010.

Lim, C. Y., Hagan, D. H., Coggon, M. M., Koss, A. R., Sekimoto, K., De Gouw, J., Warneke, C., Cappa, C. D., and Kroll, J. H.: Secondary organic aerosol formation from biomass burning emissions, Atmos. Chem. Phys. Discuss., https://doi.org/10.5194/acp-2019-326, 2019.

Lin, P., Aiona, P. K., Li, Y., Shiraiwa, M., Laskin, J., Nizkorodov, S. A., and Laskin, A.: Molecular Characterization of Brown Carbon in Biomass Burning Aerosol Particles, Environmental Science & Technology, 50, 11815-11824, https://doi.org/10.1021/acs.est.6b03024, 2016.

Liu, D. T., Whitehead, J., Alfarra, M. R., Reyes-Villegas, E., Spracklen, D. V., Reddington, C. L., Kong, S. F., Williams, P. I., Ting, Y. C., Haslett, S., Taylor, J. W., Flynn, M. J., Morgan, W. T., McFiggans, G., Coe, H., and Allan, J. D.: Black-carbon absorption enhancement in the atmosphere determined by particle mixing state, Nat. Geosci., 10, 184-U132, https://doi.org/10.1038/ngeo2901, 2017.

Liu, S., Aiken, A. C., Arata, C., Dubey, M. K., Stockwell, C. E., Yokelson, R. J., Stone, E. A., Jayarathne, T., Robinson, A. L., DeMott, P. J., and Kreidenweis, S. M.: Aerosol single scattering albedo dependence on biomass combustion efficiency: Laboratory and field studies, Geophysical Research Letters, 2013GL058392, https://doi.org/10.1002/2013GL058392, 2013.

Liu, S., Aiken, A. C., Gorkowski, K., Dubey, M. K., Cappa, C. D., Williams, L. R., Herndon, S. C., Massoli, P., Fortner, E. C., Chhabra, P. S., Brooks, W. A., Onasch, T. B., Worsnop, D. R., China, S., Sharma, N., Mazzoleni, C., Xu, L., L., N. N., Liu, D., Allan, J. D., Lee, J. D., Fleming, Z. L., Mohr, C., Zotter, P., Szidat, S., and Prevot, A. S. H.: Enhanced light absorption by mixed source black and brown carbon particles in UK winter, Nat. Comm., 6, 8435, https://doi.org/10.1038/ncomms9435, 2015.

Mann, G. W., Carslaw, K. S., Reddington, C. L., Pringle, K. J., Schulz, M., Asmi, A., Spracklen, D. V., Ridley, D. A., Woodhouse, M. T., Lee, L. A., Zhang, K., Ghan, S. J., Easter, R. C., Liu, X., Stier, P., Lee, Y. H., Adams, P. J., Tost, H., Lelieveld, J., Bauer, S. E., Tsigaridis, K., van Noije, T. P. C., Strunk, A., Vignati, E., Bellouin, N., Dalvi, M., Johnson, C. E., Bergman, T., Kokkola, H., von Salzen, K., Yu, F., Luo, G., Petzold, A., Heintzenberg, J., Clarke, A., Ogren, J. A., Gras, J., Baltensperger, U., Kaminski, U., Jennings, S. G., O'Dowd, C. D., Harrison, R. M., Beddows, D. C. S., Kulmala, M., Viisanen, Y., Ulevicius, V., Mihalopoulos, N., Zdimal, V., Fiebig, M., Hansson, H. C., Swietlicki, E., and Henzing, J. S.: Intercomparison and evaluation of global aerosol microphysical properties among AeroCom models of a range of complexity, Atmos. Chem. Phys., 14, 4679-4713, https://doi.org/10.5194/acp-14-4679-2014, 2014.

May, A. A., McMeeking, G. R., Lee, T., Taylor, J. W., Craven, J. S., Burling, I., Sullivan, A. P., Akagi, S., Collett Jr., J. L., Flynn, M., Coe, H., Urbanski, S. P., Seinfeld, J. H., Yokelson, R. J., and Kreidenweis, S. M.: Aerosol emissions from prescribed fires in the United States: A synthesis of laboratory and aircraft measurements, Journal of Geophysical Research: Atmospheres, 119, 11,826-811,849, https://doi.org/10.1002/2014JD021848, 2014.

McMeeking, G. R., Kreidenweis, S. M., Baker, S., Carrico, C. M., Chow, J. C., Collett, J. L., Hao, W. M., Holden, A. S., Kirchstetter, T. W., Malm, W. C., Moosmüller, H., Sullivan, A. P., and Wold, C. E.: Emissions of trace gases and aerosols during the open combustion of biomass in the laboratory, Journal of Geophysical Research: Atmospheres, 114, D19210, https://doi.org/10.1029/2009JD011836, 2009.

McMeeking, G. R., Fortner, E., Onasch, T. B., Taylor, J. W., Flynn, M., Coe, H., and Kreidenweis, S. M.: Impacts of nonrefractory material on light absorption by aerosols emitted from biomass burning, Journal of Geophysical Research: Atmospheres, 119, 12,272-212,286, https://doi.org/10.1002/2014JD021750, 2014.

Metcalf, A. R., Loza, C. L., Coggon, M. M., Craven, J. S., Jonsson, H. H., Flagan, R. C., and Seinfeld, J. H.: Secondary Organic Aerosol Coating Formation and Evaporation: Chamber Studies Using Black Carbon Seed Aerosol and the Single-Particle Soot Photometer, Aerosol Sci. Technol., 47, 326-347, https://doi.org/10.1080/02786826.2012.750712, 2013.

Mohr, C., Lopez-Hilfiker, F. D., Zotter, P., Prévôt, A. S. H., Xu, L., Ng, N. L., Herndon, S. C., Williams, L. R., Franklin, J. P., Zahniser, M. S., Worsnop, D. R., Knighton, W. B., Aiken, A. C., Gorkowski, K. J., Dubey, M. K., Allan, J. D., and Thornton, J. A.: Contribution of Nitrated Phenols to Wood Burning Brown Carbon Light Absorption in Detling, United Kingdom during Winter Time, Environmental Science & Technology, 47, 6316-6324, https://doi.org/10.1021/es400683v, 2013.

Onasch, T. B., Trimborn, A. M., Fortner, E. C., Jayne, J. T., Kok, G. L., Williams, L. R., Davidovits, P., and Worsnop, D. R.: Soot Particle Aerosol Mass Spectrometer: Development, Validation and Initial Application, Aerosol Science and Technology, 46, 804-817, https://doi.org/10.1080/02786826.2012.663948, 2012.

Peng, J., Hu, M., Guo, S., Du, Z., Zheng, J., Shang, D., Zamora, M. L., Zeng, L., Shao, M., Wu, Y.-S., Zheng, J., Wang, Y., Glen, C. R., Collins, D. R., Molina, M. J., and Zhang, R.: Markedly enhanced absorption and direct radiative forcing of black carbon under polluted urban environments, Proc. Natl. Acad. Sci. U. S. A., 113, 4266-4271, https://doi.org/10.1073/pnas.1602310113, 2016.

Phillips, S. M., and Smith, G. D.: Spectroscopic comparison of water- and methanol-soluble brown carbon particulate matter, Aerosol Science and Technology, 51, 1113-1121, https://doi.org/10.1080/02786826.2017.1334109, 2017.

Pokhrel, R. P., Wagner, N. L., Langridge, J. M., Lack, D. A., Jayarathne, T., Stone, E. A., Stockwell, C. E., Yokelson, R. J., and Murphy, S. M.: Parameterization of single-scattering albedo (SSA) and absorption Ångström exponent (AAE) with EC / OC for aerosol emissions from biomass burning, Atmos. Chem. Phys., 16, 9549-9561, https://doi.org/10.5194/acp-16-9549-2016, 2016.

Pokhrel, R. P., Beamesderfer, E. R., Wagner, N. L., Langridge, J. M., Lack, D. A., Jayarathne, T., Stone, E. A., Stockwell, C. E., Yokelson, R. J., and Murphy, S. M.: Relative importance of black carbon, brown carbon, and absorption enhancement from clear coatings in biomass burning emissions, Atmospheric Chemistry and Physics, 17, 5063-5078, https://doi.org/10.5194/acp-17-5063-2017, 2017.

Qin, Y. M., Tan, H. B., Li, Y. J., Li, Z. J., Schurman, M. I., Liu, L., Wu, C., and Chan, C. K.: Chemical characteristics of brown carbon in atmospheric particles at a suburban site near Guangzhou, China, Atmos. Chem. Phys., 18, 16409-16418, https://doi.org/10.5194/acp-18-16409-2018, 2018.

Reid, J. S., Koppmann, R., Eck, T. F., and Eleuterio, D. P.: A review of biomass burning emissions part II: intensive physical properties of biomass burning particles, Atmos. Chem. Phys., 5, 799-825, https://doi.org/10.5194/acp-5-799-2005, 2005.

Sahu, L. K., Kondo, Y., Moteki, N., Takegawa, N., Zhao, Y., Cubison, M. J., Jimenez, J. L., Vay, S., Diskin, G. S., Wisthaler, A., Mikoviny, T., Huey, L. G., Weinheimer, A. J., and Knapp, D. J.: Emission characteristics of black carbon in anthropogenic and biomass burning plumes over California during ARCTAS-CARB 2008, Journal of Geophysical Research-Atmospheres, 117, https://doi.org/10.1029/2011jd017401, 2012.

Saleh, R., Hennigan, C. J., McMeeking, G. R., Chuang, W. K., Robinson, E. S., Coe, H., Donahue, N. M., and Robinson, A. L.: Absorptivity of brown carbon in fresh and photo-chemically aged biomass-burning emissions, Atmospheric Chemistry and Physics, 13, 7683-7693, https://doi.org/10.5194/acp-13-7683-2013, 2013.

Saleh, R., Robinson, E. S., Tkacik, D. S., Ahern, A. T., Liu, S., Aiken, A. C., Sullivan, R. C., Presto, A. A., Dubey, M. K., Yokelson, R. J., Donahue, N. M., and Robinson, A. L.: Brownness of organics in aerosols from biomass burning linked to their black carbon content, Nature Geosci, 7, 647-650, https://doi.org/10.1038/ngeo2220, 2014.

Saleh, R., Cheng, Z., and Atwi, K.: The Brown–Black Continuum of Light-Absorbing Combustion Aerosols, Environmental Science & Technology Letters, ASAP, https://doi.org/10.1021/acs.estlett.8b00305, 2018.

Schneider, J., Weimer, S., Drewnick, F., Borrmann, S., Helas, G., Gwaze, P., Schmid, O., Andreae, M. O., and Kirchner, U.: Mass spectrometric analysis and aerodynamic properties of various types of combustion-related aerosol particles, International Journal of Mass Spectrometry, 258, 37-49, https://doi.org/10.1016/j.ijms.2006.07.008, 2006.

Schwarz, J. P., Gao, R. S., Spackman, J. R., Watts, L. A., Thomson, D. S., Fahey, D. W., Ryerson, T. B., Peischl, J., Holloway, J. S., Trainer, M., Frost, G. J., Baynard, T., Lack, D. A., de Gouw, J. A., Warneke, C., and Del Negro, L. A.: Measurement of the mixing state, mass, and optical size of individual black carbon particles in urban and biomass burning emissions, Geophysical Research Letters, 35, L13810, https://doi.org/10.1029/2008gl033968, 2008.

Sekimoto, K., Koss, A. R., Gilman, J. B., Selimovic, V., Coggon, M. M., Zarzana, K. J., Yuan, B., Lerner, B. M., Brown, S. S., Warneke, C., Yokelson, R. J., Roberts, J. M., and de Gouw, J.: High- and low-temperature pyrolysis profiles describe volatile organic compound emissions from western US wildfire fuels, Atmos. Chem. Phys., 18, 9263-9281, https://doi.org/10.5194/acp-18-9263-2018, 2018.

Sengupta, D., Samburova, V., Bhattarai, C., Kirillova, E., Mazzoleni, L., Iaukea-Lum, M., Watts, A., Moosmüller, H., and Khlystov, A.: Light absorption by polar and non-polar aerosol compounds from laboratory biomass combustion, Atmos. Chem. Phys., 18, 10849-10867, https://doi.org/10.5194/acp-18-10849-2018, 2018.

Shamjad, P. M., Tripathi, S. N., Thamban, N. M., and Vreeland, H.: Refractive Index and Absorption Attribution of Highly Absorbing Brown Carbon Aerosols from an Urban Indian City-Kanpur, Scientific Reports, 6, 37735, https://doi.org/10.1038/srep37735, 2016.

Shiraiwa, M., Kondo, Y., Iwamoto, T., and Kita, K.: Amplification of Light Absorption of Black Carbon by Organic Coating, Aerosol Science and Technology, 44, 46-54, https://doi.org/10.1080/02786820903357686, 2010.

Sumlin, B. J., Pandey, A., Walker, M. J., Pattison, R. S., Williams, B. J., and Chakrabarty, R. K.: Atmospheric Photooxidation Diminishes Light Absorption by Primary Brown Carbon Aerosol from Biomass Burning, Environmental Science & Technology Letters, 4, 540-545, https://doi.org/10.1021/acs.estlett.7b00393, 2017.

Sumlin, B. J., Heinson, Y. W., Shetty, N., Pandey, A., Pattison, R. S., Baker, S., Hao, W. M., and Chakrabarty, R. K.: UV–Vis–IR spectral complex refractive indices and optical properties of brown carbon aerosol from biomass burning, Journal of Quantitative Spectroscopy and Radiative Transfer, 206, 392-398, https://doi.org/10.1016/j.jqsrt.2017.12.009, 2018.

Wandinger, Ulla, Müller, Detlef, Böckmann, Christine, Althausen, Dietrich, Matthias, Volker, Bösenberg, Jens, Weiß, Volker, Fiebig, Markus, Wendisch, Manfred, Stohl, Andreas, and Ansmann, A.: Optical and microphysical characterization of biomass- burning and industrial-pollution aerosols from- multiwavelength lidar and aircraft measurements, Journal of Geophysical Research: Atmospheres, 107, LAC 7-1-LAC 7-20, https://doi.org/doi:10.1029/2000JD000202, 2002.

Washenfelder, R. A., Attwood, A. R., Brock, C. A., Guo, H., Xu, L., Weber, R. J., Ng, N. L., Allen, H. M., Ayres, B. R., Baumann, K., Cohen, R. C., Draper, D. C., Duffey, K. C., Edgerton, E., Fry, J. L., Hu, W. W., Jimenez, J. L., Palm, B. B., Romer, P., Stone, E. A., Wooldridge, P. J., and Brown, S. S.: Biomass burning dominates brown carbon absorption in the rural southeastern United States, Geophysical Research Letters, 42, 653-664, https://doi.org/10.1002/2014GL062444, 2015.

Xie, M., Hays, M. D., and Holder, A. L.: Light-absorbing organic carbon from prescribed and laboratory biomass burning and gasoline vehicle emissions, Scientific Reports, 7, 7318, https://doi.org/10.1038/s41598-017-06981-8, 2017.

Yang, M., Howell, S. G., Zhuang, J., and Huebert, B. J.: Attribution of aerosol light absorption to black carbon, brown carbon, and dust in China – interpretations of atmospheric measurements during EAST-AIRE, Atmospheric Chemistry and Physics, 9, 2035-2050, https://doi.org/10.5194/acp-9-2035-2009, 2009.

Zhang, X., Kim, H., Parworth, C., Young, D. E., Zhang, Q., Metcalf, A. R., and Cappa, C. D.: Optical Properties of Wintertime Aerosols from Residential Wood Burning in Fresno, CA: Results from DISCOVER-AQ 2013, Environmental Science & Technology, 50, 1681-1690, https://doi.org/10.1021/acs.est.5b04134, 2016.

9 Tables

Table 1. Fuels by particle Class.

Class	Fuel	SSA range	[OA]/[BC] range
Class 1	Chaparral, canopy, litter (pine), building materials, excelsior	0.23-0.43	0.3-2.4
Class 2	Manzanita, Sage, litter (fir)	0.43-0.60	1.5-4.1
Type 3	Pine, fir, litter, canopy, juniper	0.60-0.74	6.6-20
Class 4	Pine, fir, canopy, rotten log, ceonothos	0.74-0.87	8.3-55
Class 5	Canopy (pine), rice, bear grass, duff	0.87-0.93	31-143
Class 6	Rotten log, duff, peat, dung	0.93-1.00	431-10^5

10 Figures

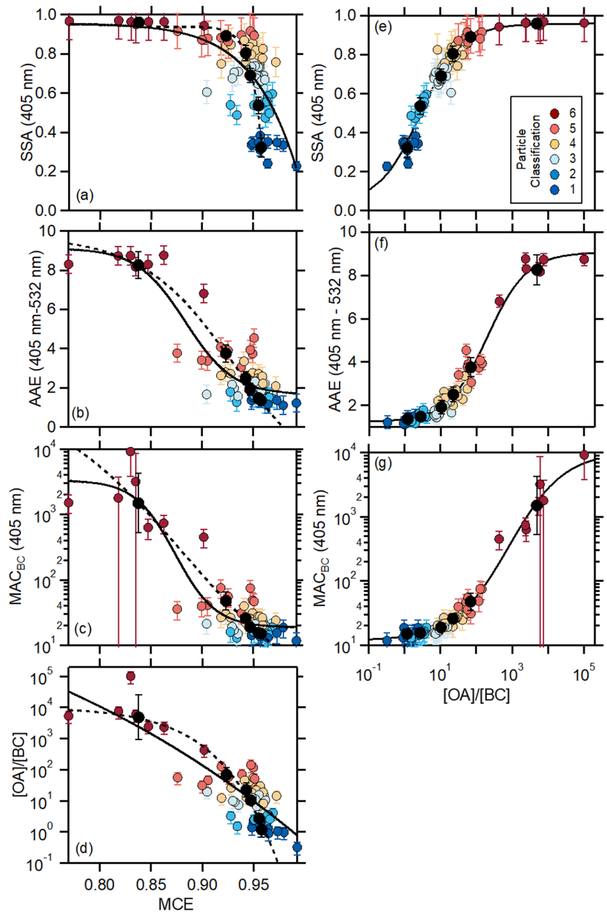

Figure 1. (left panels) Relationship between (a) the SSA_{405nm}, (b) the $AAE_{405-532}$, (c) the MAC_{BC}, and (d) the [OA]/[BC] mass ratio and the modified combustion efficiency, MCE. Results for individual burns are shown as points colored by the particle Class, and Class average values are shown as black circles. Uncertainties on the Class averages are 1σ based on measurement variability and uncertainties on for the individual burns are from error propagation of measurement uncertainties. The solid black lines are fits to the individual burns (colored points) while the dashed black lines are fits to the Class averages (Table S2). (right panels) Relationship between (e) the SSA_{405nm}, (f) the $AAE_{405-532}$, and (g) the MAC_{BC} on the [OA]/[BC] mass ratio. The solid black lines here are sigmoidal fits to the individual burns. Fits to the Class averages are similar.

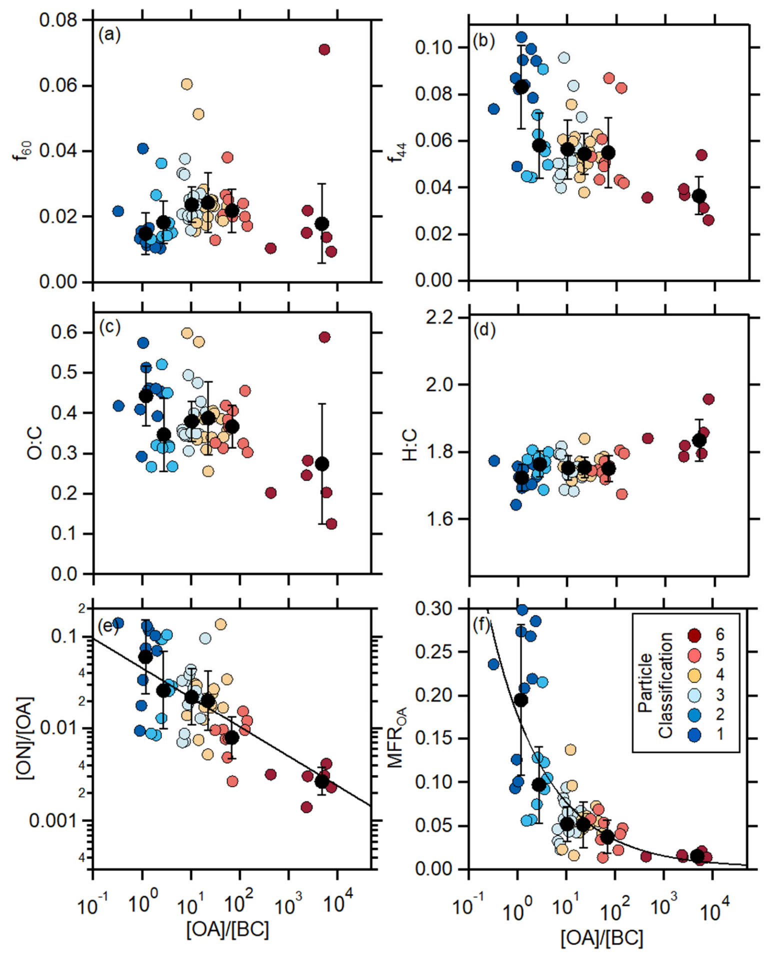

Figure 2. Dependence of (a) f_{60}, (b) f_{44}, (c) O:C, (d) H:C, (e) the nitrated organic fraction of OA, $f_{ON\text{-}OA}$, and (f) the OA volatility, characterized as the mass fraction remaining after heating. Results for individual burns are shown as points colored by the particle Class, and Class average values are shown as black circles. Uncertainties on the Class averages are 1σ based on measurement variability. For $f_{ON\text{-}OA}$ and MFR_{OA}, fits to the observations are shown (see text).

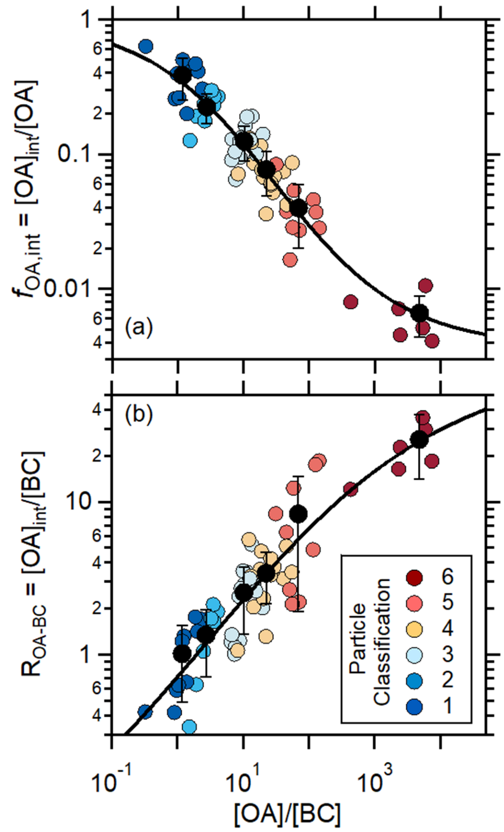

Figure 3. Relationship between (a) the fraction of OA that is internally mixed with BC, $f_{OA,int}$ and (b) the OA-to-BC mass ratio for only the internally mixed OA, and the total [OA]/[BC] mass ratio. Results for individual burns are shown as points colored by the particle Class, and Class average values are shown as black circles. Uncertainties on the Class averages are 1σ based on measurement variability. Black lines are sigmoidal fits to the data, in log-log space.

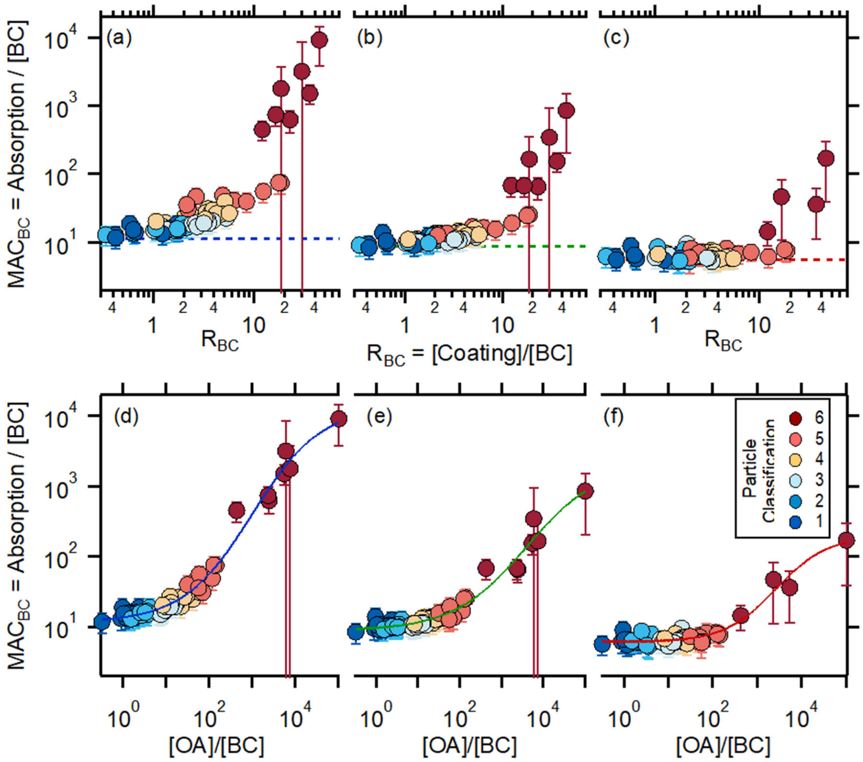

Figure 4. (Top Panels) The relationship between the wavelength-specific MAC_{BC} and the coating-to-BC mass ratio for (a) 405 nm, (b) 532 nm and (c) 781 nm. The horizontal dashed lines show the derived $MAC_{BC,pure}$ values. (Bottom Panels) The relationship between the wavelength-dependent MAC_{BC} and the total [OA]/[BC] mass ratio for (d) 405 nm, (e) 532 nm and (f) 781 nm. The lines are sigmoidal fits. Uncertainties for the individual burns are determined from error propagation. Graphs of the wavelength-specific MAC_{BC} versus [OA]/[BC] with each shown using independent y-axis scales are provided for comparison in **Figure S1**.

Deleted: dependent

Deleted: a

Deleted: b

Deleted: c

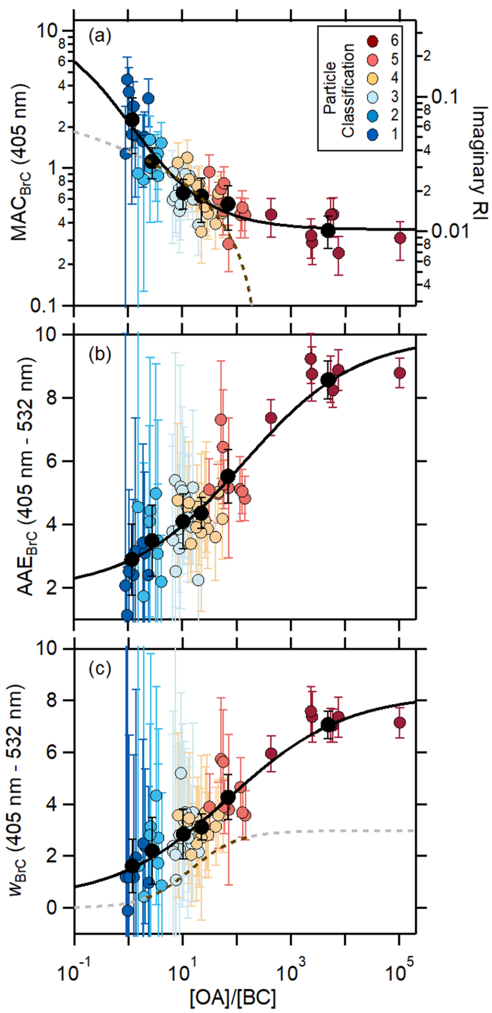

Figure 5. Relationship between (a) $MAC_{\mathrm{BrC,405nm}}$, (b) $AAE_{\mathrm{BrC,405\text{-}532}}$, and (c) $w_{\mathrm{BrC,405\text{-}532}}$ and the [OA]/[BC] mass ratio. The solid lines are sigmoidal fits to the observations, against log([OA]/[BC]). The dashed lines are based on the parameterization of Saleh et al. (2014), with the brown color indicating the measuring range in that study and the gray color extrapolated. Results for individual burns are shown as points colored by the particle Class, and Class average values are shown as black circles. Uncertainties on the Class averages are 1σ based on measurement variability. Uncertainties for the individual burns are determined from error propagation.

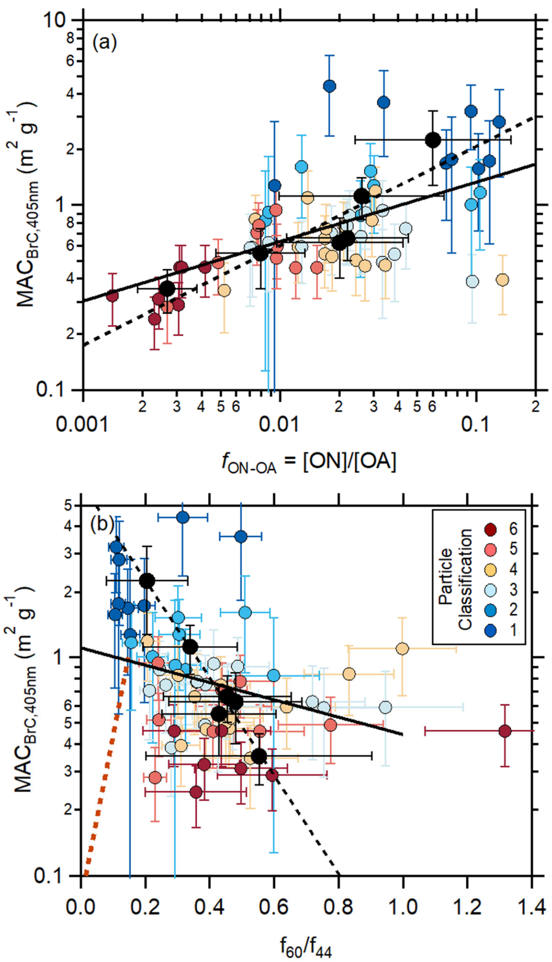

Figure 6. Relationship between the $MAC_{BrC,405nm}$ and (a) the nitrated organic fraction of total organic aerosol, f_{ON-OA}, and (b) the f_{60}/f_{44} ion ratio for organic aerosol. Results for individual burns are shown as points colored by the particle Class, and Class average values are shown as black circles. Uncertainties on the Class averages are 1σ based on measurement variability. Uncertainties for the individual burns are determined from error propagation. Solid black lines are fits to all burns and dashed black lines are fits to the Class averages. The dashed brown line in panel (b) is the relationship reported by Lack et al. (2013) for ambient particles in a biomass burning plume.

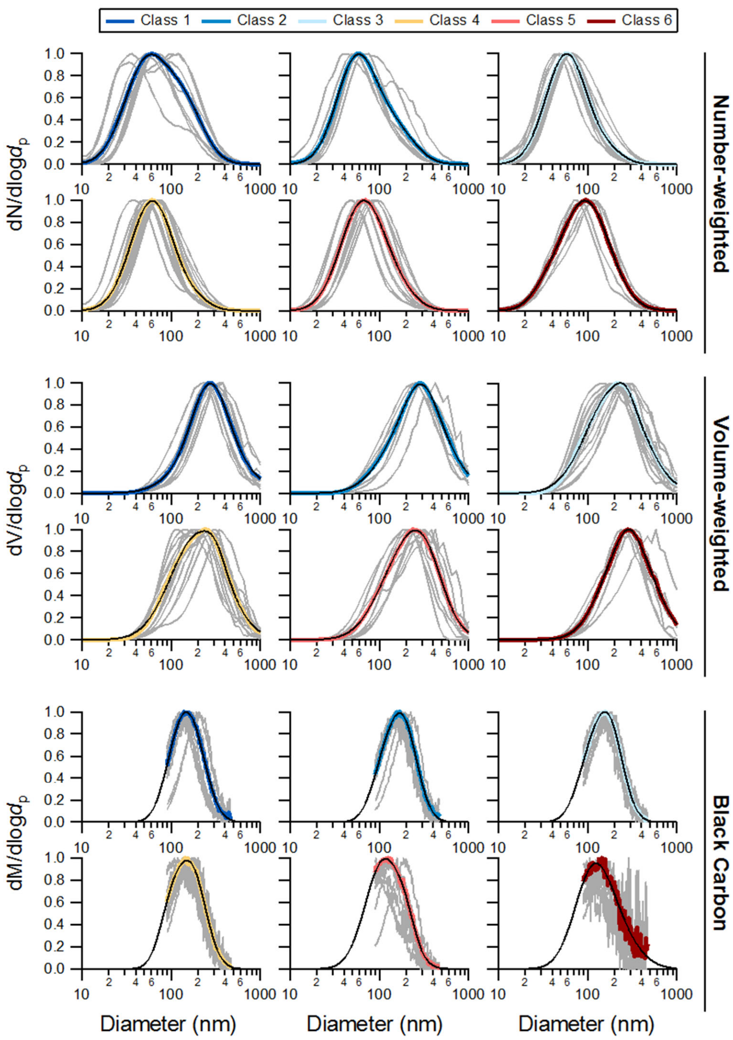

Figure 7. Class-specific total particle number-weighted (top) and volume-weighted (middle) mobility size distributions, and the BC-only mass-weighted (bottom) size distribution. Individual burns are shown in gray and class averages are shown as colors. Bimodal log-normal fits are thin black lines. Note that the number-weighted and volume-weighted distributions are graphed versus mobility diameter and the BC mass-weighted distribution against the BC volume equivalent diameter.

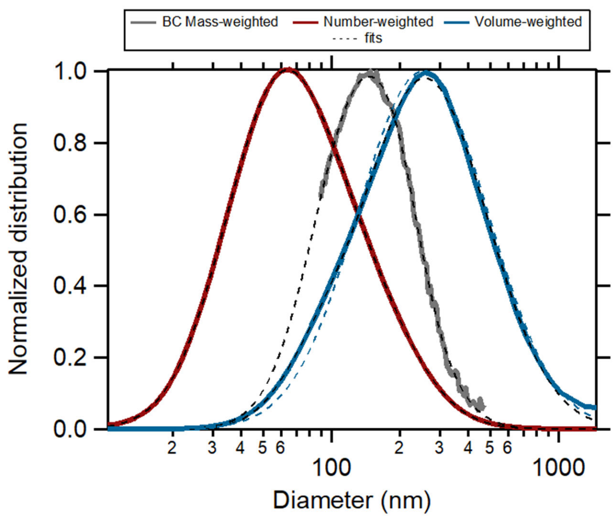

Figure 8. Average total particle number-weighted (red) and volume-weighted (blue) size distributions and the BC-specific mass-weighted size distributions. Black dashed lines are bimodal log-normal fits. The dashed blue line is the total particle volume-weighted distribution calculated from a single-mode fit to the number-weighted distribution. Note that the number-weighted and volume-weighted distributions are graphed versus mobility diameter and the BC mass-weighted distribution against the BC volume equivalent diameter.

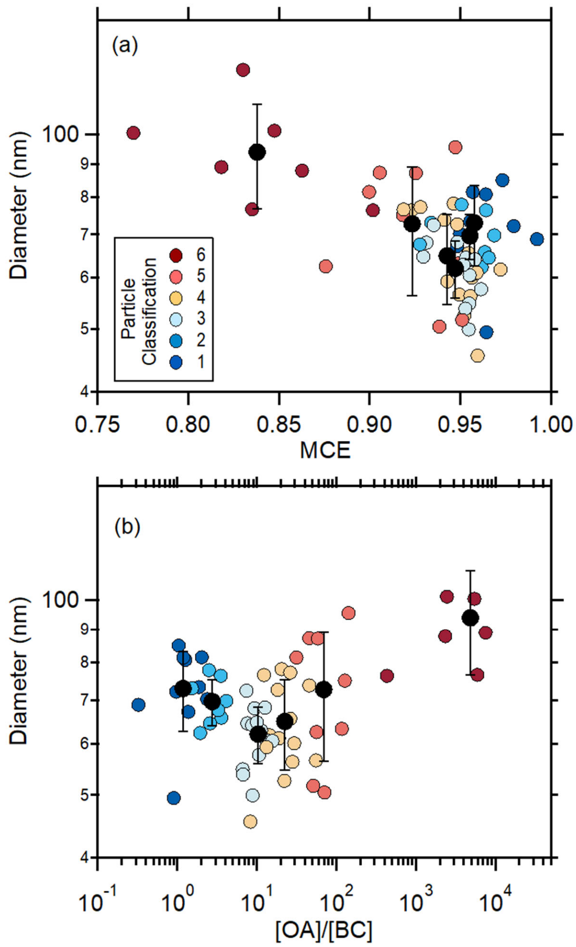

Figure 9. Relationship between number-weighted particle median diameter and (a) the MCE and (b) the [OA]/[BC] ratio. Colored circles are for individual burns and black circles for particle class averages.

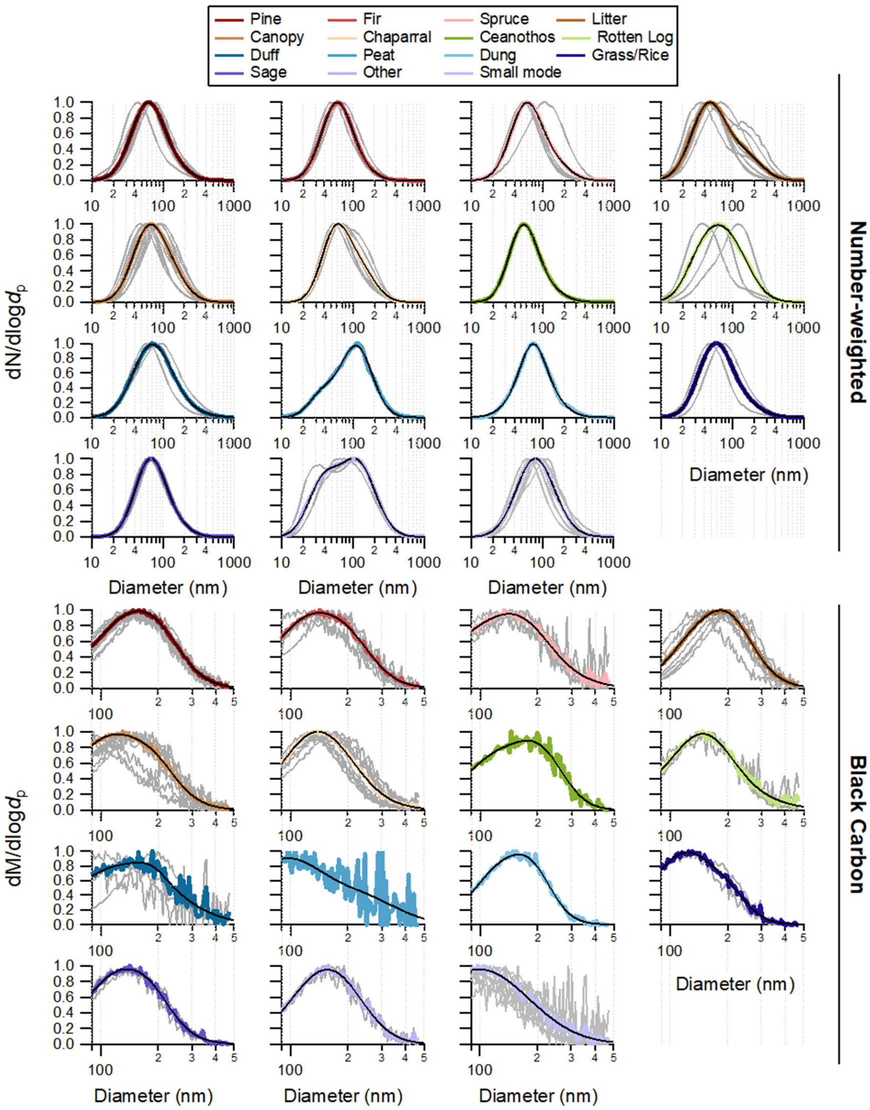

Figure 10. Normalized total particle number-weighted (top) and the BC-only mass-weighted (bottom) size distributions shown by fuel type (see legend). Individual burns are gray and averages for a fuel type colors. For some fuels there is only one size distribution. Bimodal log-normal fits are the black lines. The "other" category includes non-traditional biofuels, specifically building materials and excelsior.

Supplementary Material for:

Biomass-burning derived particles from a wide variety of fuels: Part 1: Properties of primary particles

Crystal D. McClure[1], Christopher Y. Lim[2,%], David H. Hagan[2], Jesse H. Kroll[2], Christopher D. Cappa[1,3,*]

[1] Department of Civil and Environmental Engineering, University of California, Davis, CA 95616

[2] Department of Civil and Environmental Engineering, Massachusetts Institute of Technology, Cambridge, MA, USA

[3] Atmospheric Sciences Graduate Group, University of California, Davis, CA, USA 95616

[%] Now at Department of Chemistry, University of Toronto, Ontario, Canada

[*] To whom correspondence should be addressed: cdcappa@ucdavis.edu

10.1 Description of Instrumentation

Particle Optical Property Measurements

Particle optical properties for PM_1 were measured at 405 nm and 532 nm using the UC Davis Cavity Ringdown-Photoacoustic Spectrometer (CRD-PAS). In the UC Davis CRD-PAS, Light absorption coefficients (b_{abs}; units = Mm^{-1}) for dry particles are determined using photoacoustic spectroscopy (Lack et al., 2012b). Light extinction coefficients (b_{ext}; units = Mm^{-1}) for dry (<20% relative humidity) particles are measured at 405 nm and 532 nm via cavity ringdown spectroscopy (Langridge et al., 2011). Humidified light extinction measurements (RH ~85%) are also measured at 532 nm by cavity ringdown spectroscopy. The absorption measurements from the PAS were calibrated relative to the extinction measurement from the CRD using gas-phase O_3 and NO_2 with an estimated accuracy of 5% at 532 nm and 8% at 405 nm. Light absorption and scattering coefficients were also measured at 781 nm using a commercial PASS-3 photoacoustic spectrometer (DMT, Inc.). In the PASS-3, light absorption coefficients are measured by photoacoustic spectroscopy. Light scattering coefficients (b_{sca}; units = Mm^{-1}) are determined for dry particles with the PASS-3 using reciprocal nephelometry. The absorption measured by the

PASS-3 was calibrated relative to the UC Davis PAS using polydisperse fullerene soot and assuming that the absorption Ångstrom exponent was 1.4 (Metcalf et al., 2013). The estimated uncertainty in b_{abs} at 781 nm is 10%.

Particle Composition Measurements

Refractory black carbon measurement

Refractory black carbon (rBC) concentrations and BC-specific particle size distributions were measured using a single particle soot photometer (SP2). The SP2 measures the concentration of rBC within individual rBC-containing particles. Sampled particles pass through a 1064 nm intracavity laser. Absorption of this light by rBC leads to rapid heating of the particles. If heating outweighs conductive cooling the particles will reach a sufficiently high temperature (i.e. their boiling point) that they will incandesce. The intensity of this incandescent light is proportional to the rBC mass of that particle (usually on the order of 0.1 – 10 fg per particle). Size distributions of only the rBC (exclusive of any other internally mixed material) are generated by converting the per particle mass to a volume equivalent diameter ($d_{p,VED}$ here, assuming ρ_{rBC} = 1.8 g cm^{-3}) and binning the particles by size. The SP2 was calibrated using size-selected fullerene particles (Lot L20W054, Alfa Aesar, Ward Hill, MA, USA).

When the number concentration of rBC-containing or non-rBC-containing particles is large, the SP2 may suffer from negative biases in the concentration measurement. This can happen when the SP2 detectors are triggered by one particle and a second passes through the viewing volume during the detection window (typically ~50 μs). Such particle coincidence effects can be minimized by decreasing the sample flowrate into the SP2 to decrease the likelihood that two particles are simultaneously in the viewing volume. Here, the SP2 sample flowrate was varied from 5 sccm to 120 sccm in a step-wise manner over the course of an experiment to deal with the very large dynamic range of concentrations in the mini chamber. The flow rate was increased to maintain an approximately constant particle count rate in the instrument while minimizing the influence of particle coincidence. Inspection of individual particle detection events indicates that particle coincidence was generally avoided.

The SP2 data were processed using the SP2 Toolkit from the Paul Scherer Institute (PSI), developed by Martin Gysel. The SP2 size-dependent counting efficiency was determined by simultaneously measuring the concentration of the calibration particles with a mixing condensation particle counter (BMI Model 2002). The particle counting efficiency was found to be unity for particles with $d_{p,VED}$ > 100 nm. The SP2 used in this study measured particles over the size range $90 \leq d_{p,VED} \leq 822$. Below the lower size limit, the detection efficiency falls off rapidly due, in part, to the large surface area-to-volume (SA-to-V) ratio of these particles. When the SA-to-V ratio is sufficiently large conductive cooling competes effectively with the radiative heating from the laser and the particles do not emit enough incandescent light at short enough wavelengths to trigger detection. Above the upper size limit, the incandescence level is sufficient to saturate the detector, leading to an underestimate in particle mass. All SP2 mass concentration measurements were corrected for the missing mass contained in particles below the lower and upper size limit, using a multi-mode fitting approach.

The observed campaign average distribution mode peak is around 150 nm. The observed distributions (1 min averages) were fit to a four-mode log-normal distribution to estimate and correct for the rBC outside of the SP2 detection window, i.e. for rBC "missing mass". The average ratio between the observed rBC concentration and the total estimated from fitting was 0.83 ± 0.06 (1σ). There was some experiment-to-experiment and time-dependent variability in the missing mass fraction that is accounted for by fitting the observations at 1 min time resolution. This approach follows that of Zhang et al. (2016). While a single mode fit provides a reasonably representation of the overall campaign average distribution, inspection of the individual distributions across the experiments indicates that a multi-mode fitting approach provides a substantially more robust description of the observed size distribution, especially as particle aging proceeds.

Composition and concentration of NR-PM

The concentration of non-refractory particulate matter (NR-PM) species in PM_1 were measured using a high-resolution time-of-flight aerosol mass spectrometer (HR-ToF-AMS, henceforth HR-AMS) (Canagaratna et al., 2007) during both the Fresno and Fontana studies, as discussed in detail by (Lim et al., 2019). The NR-PM components are functionally defined as those materials that evaporate rapidly after impaction onto a heated surface *in vacuo* at ~600 °C. The NR-PM components characterized include particulate sulfate, nitrate, ammonium, chloride and organic matter. The data were processed using the PIKA toolkit in IGOR (Wavemetrics, Inc.). The collection efficiency (CE) of the HR-AMS was determined by comparison with size distributions measured using the scanning electrical mobility spectrometer (SEMS). The collection efficiency differed between primary and secondary and secondary particles and was found to co-vary with the volatility of the organic aerosol. The variation in the CE was empirically accounted for, as discussed in (Lim et al., 2019). The estimated uncertainty for the HR-AMS measurements is ±30%, although the precision is much better than this.

Particulate nitrated organics characterization

The concentration of nitrated organic functional groups (ON_f) is determined from the HR-AMS measurements. Kiendler-Scharr et al. (2016) showed that the fraction of total nitrate measured by the HR-AMS that derives from organic nitrate functional groups ($f_{ON\text{-}N}$) relates to the measured $[NO_2^+]/[NO^+]$ ratio (R_{meas}):

$$f_{ON-N} = \frac{(1+R_{ON})\cdot(R_{meas}-R_{calib})}{(1+R_{meas})\cdot(R_{ON}-R_{calib})} \qquad \text{(S1)}$$

where R_{ON} = 0.1 and R_{calib} is an instrument-specific factor determined from calibration with NH_4NO_3 and here equaling 0.45. The Kiendler-Scharr et al. (2016) approach focused on the behavior of organic nitrates. We assume here that nitro-organics behave similarly and thus that ON_f encompasses contributions from both nitrate and nitro functional groups. Equation S1 is thought reliable when the $f_{ON\text{-}N} > 0.15$ (Bruns et al., 2010). The average $f_{ON\text{-}N}$ for the FIREX measurements is 0.74 ± 0.24 (1σ). The concentration of particulate ON functional groups is then $[ON_f] = f_{ON\text{-}N}\cdot[NO_3^-]$. Note that this includes only the mass of the functional group; the total mass concentration of the ON species (including the carbon backbone) can be estimated by multiplying the ON_f concentration by the ratio between an assumed MW for the ON species and that for the nitrate functional group. We assume that ON species have a MW = 200 amu, and thus [ON] = $3.22\cdot[ON_f]$. If the ON signal is dominated by nitro functional groups, rather than nitrate, then the estimated [ON] is a lower limit.

Composition and concentration of BC-containing particles

The concentrations and composition of only BC-containing particles were determined using a soot particle aerosol mass spectrometer (SP-AMS) (Onasch et al., 2012). In the SP-AMS, a focused particle beam is intersected with an intra-cavity Nd:YAG laser operating at 1064 nm. Particles containing BC are rapidly heated by the laser, leading to evaporation of both the NR-PM materials and the refractory BC. In these studies, the standard HR-AMS tungsten vaporizer was removed so that particles that do not contain BC are not vaporized and are therefore not detected. Thus, the SP-AMS is specific to BC-containing particles, as operated here. In addition to BC, the SP-AMS measures the internally mixed particulate inorganic (sulfate, nitrate, ammonium, and chloride) and organic mass loading. The NR-PM species that are associated with BC will be distinguished from the bulk average NR-PM species (from the HR-AMS) using the subscript BC (i.e. NR-PM_{rBC}). The SP-AMS particle detection efficiency is determined in large part by the extent of overlap between the particle and laser beam. Particles were sampled through a PM_1 aerodynamic lens, with particles measured down to ~40 nm vacuum aerodynamic diameter. The SP-AMS detection efficiency was determined by referencing the rBC concentration measured by the SP-AMS to that measured by the SP2, as in (Collier et al., 2018). The SP-AMS/SP2 ratio depended on the ratio between the NR-PM_{BC} and BC, with the NR-PM/rBC ratio decreasing as the SP-AMS/SP2 ratio increases. However, throughout this work we use only the [NR-PM_{rBC}]/[rBC] or [OA_{rBC}]/[rBC] ratios, which are not dependent on the absolute instrument calibration, but only the relative detection efficiency of these species. The coating-to-core mass ratio for both campaigns is calculated directly from the SP-AMS measurements as R_{BC} = $[NR\text{-}PM]_{BC}$/[BC].

Gas Composition Measurements

The concentrations of select gas-phase non-methane organic gases (NMOG) and some inorganic species (e.g. HONO) were measured using H_3O^+ and I^- chemical ionization mass spectrometers (CIMS), that included high-resolution time-of-flight mass spectrometers. Only the measurements from the PTR-TOF-MS, operated by the National Oceanic and Atmospheric Administration, are used here. The PTR-TOF-MS measurements are described in detail in (Koss et al., 2018) and (Sekimoto et al., 2018). In addition to the NMOG measurements, other inorganic gases (O_3, CO, CO_2, SO_2) were measured using commercial instrumentation.

10.2 Supplemental Figures & Tables

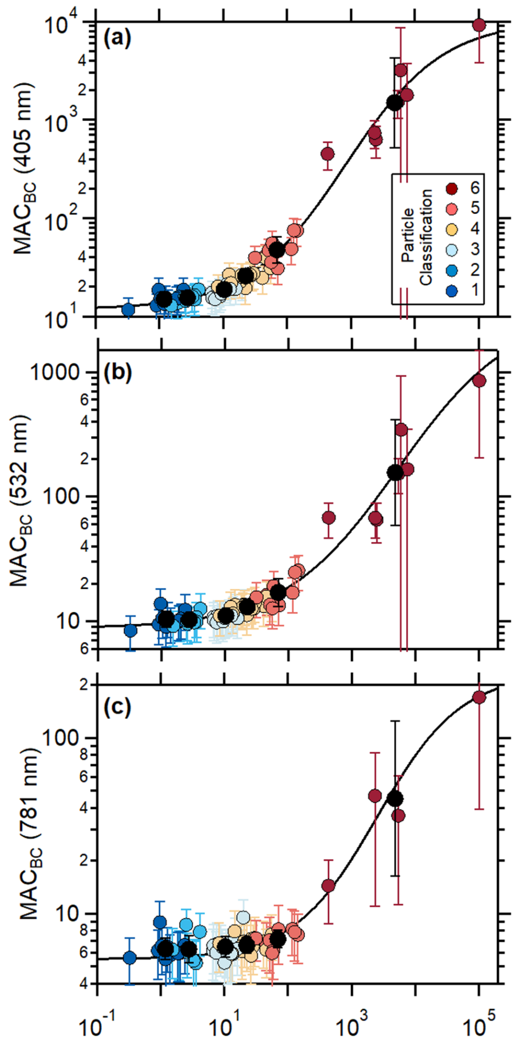

Figure S1. Relationship between the observed ambient particle MAC_{BC} and the total particle [OA]/[rBC] at (a) 405 nm, (b) 532 nm, and (c) 781 nm. Individual points colored by Class (see text) and class averages as black circles.

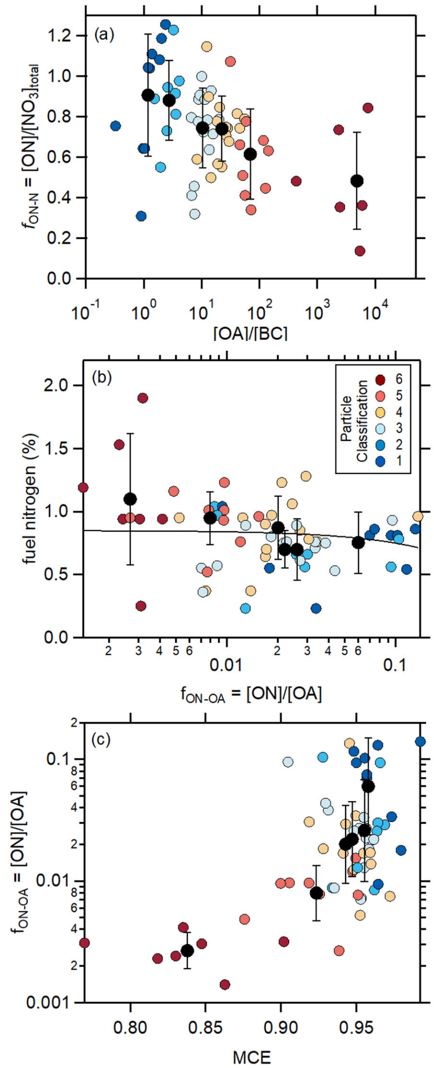

Figure S2. (a) Relationship between fuel nitrogen and the fraction of OA that is organic nitrate, $f_{ON\text{-}N}$. There is no correlation between the two. (b) Relationship between $f_{ON\text{-}OA}$ and the modified combustion efficiency, MCE. Results for individual burns are shown as points colored by the particle Class, and Class average values are shown as black circles. Uncertainties on the Class averages are 1σ based on measurement variability.

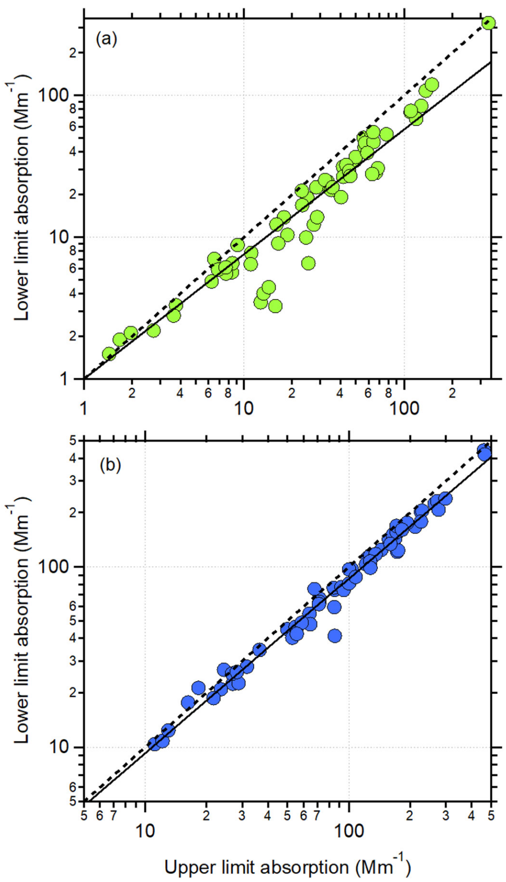

Figure S3. The derived lower limit brown carbon absorption versus the upper limit brown carbon absorption at (a) 532 nm and (b) 405 nm. The lower limit estimate for BrC absorption accounts for the potential influence of coating-induced enhancements. The dashed line is the one-to-one line and the solid line is a linear fit with slopes equaling 0.88 at 532 nm and 0.97 at 405 nm.

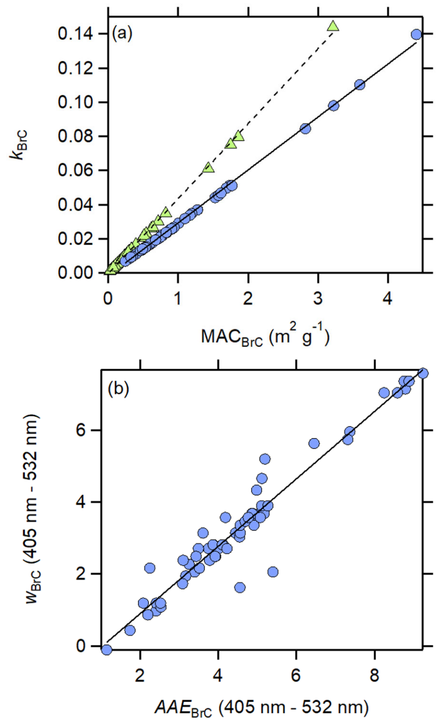

Figure S4. (a) Relationship between the imaginary refractive index for BrC, k_{BrC}, at 405 nm (blue circles) and the observed MAC_{BrC} at 405 nm or at 532 nm (green triangles). Lines are linear fits to the observations. (b) Relationship between the wavelength dependence of k_{BrC}, w_{BrC}, determined for the 405 nm – 532 nm pair, and the AAE_{BrC} for the same wavelengths.

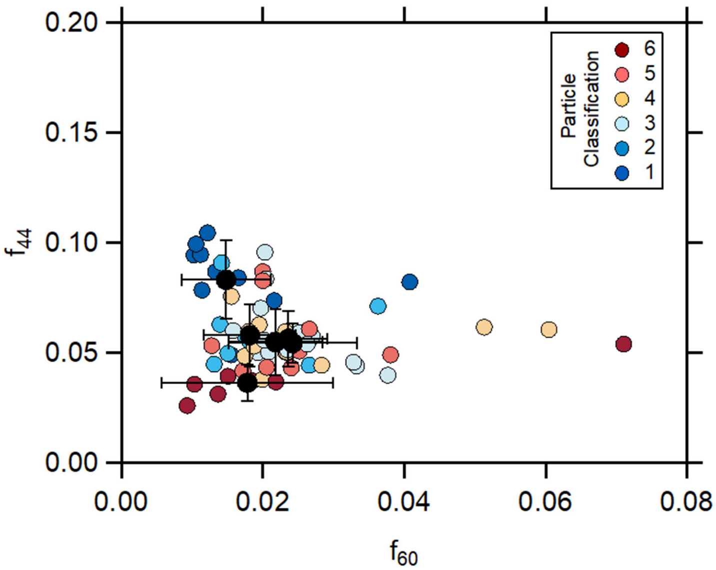

Figure S5. The relationship between the fractional abundance of the *m*/*z* = 44 (f_{44}) and *m*/*z* = 60 (f_{60}) ions from organic aerosol. Points are colored by particle class for individual burns, and the class averages shown in black.

Table S1. Fuels combusted. Further details regarding fuel properties are available at the NOAA data repository, in particular in the summary spreadsheet (https://esrl.noaa.gov/csd/groups/csd7/measurements/2016firex/FireLab/DataDownload/FIREX_BurnListComplete_V5.xlsx; access date 04 February 2019)

Fuel Type
Bear Grass
Building Material - Untreated Wood
Ceanothos
Chapparral (canopy)
Chamise
Manzanita
Douglas Fir (litter, canopy, mixture, rotten log)
Dung
Engelmann spruce (canopy, mixture, duff)
Excelsior (wood wool)
Jeffrey Pine (duff)
Juniper (canopy)
Loblolly pine (litter)
Lodgepole (canopy, litter, mixture)
Peat
Ponderosa pine (litter, canopy, mixture, rotten log)
Rice Straw, Arkansas
Sage
Sage Brush
Subalpine fir (canopy, litter, mix, duff)

Table S2. Fit coefficients for the various fits performed, organized by fit type (e.g. sigmoidal, power law, linear, exponential). Note: continues on second page.

y	x	c1	c2	c3	c4	r^2
$y = c_1 + \frac{c_2}{1+\frac{\exp(c_3 - x)}{c_4}}$						
SSA_{405nm}	log([OA]/[BC])	0.03	0.93	0.444	0.579	
SSA_{532nm}	log([OA]/[BC])	0.085	0.91	0.623	0.520	
SSA_{781nm}	log([OA]/[BC])	0.10	0.90	0.700	0.538	
$AAE_{405\text{-}532}$	log([OA]/[BC])	1.25	7.81	2.298	0.554	
$\log(MAC_{BC,405nm})$	log([OA]/[BC])	1.072	2.94	2.914	0.765	
$\log(MAC_{BC,532nm})$	log([OA]/[BC])	0.94	2.56	3.721	0.900	
$\log(MAC_{BC,781nm})$	log([OA]/[BC])	0.74	1.62	3.411	0.655	
$\log(f_{OA,int})$	log([OA]/[BC])	0	-2.43	1.477	0.987	
$\log(R_{OA,BC})$	log([OA]/[BC])	-1.76	3.70	0.462	1.823	
$\log(MAC_{BrC,405nm})$	log([OA]/[BC])	1.072	-1.519	0.053	0.732	
AAE_{405nm}	MCE	9.124	-7.476	0.884	0.0236	
AAE_{405nm}	MCE*	9.723	-13.142	0.932	0.0452	
$\log(MAC_{BC,405nm})$	MCE	3.523	-2.251	0.874	0.0198	
$\log(MAC_{BC,405nm})$	MCE*	4.949	-5.073	0.882	0.0705	
log([OA]/[BC])	MCE*	4.030	-39.57	1.072	0.0500	
$y = c_1 + c_2 \cdot x^{c_3}$						
SSA_{405nm}	MCE	0.954	-0.880	22.76		
SSA_{405nm}	MCE*	0.939	-26.34	88.29		
log([OA]/[BC])	MCE	7.952	-8.272	3.351		
$y = c_1 \cdot x + c_2$						
f_{44}	log([OA]/[BC])	-0.0097	0.0686			0.33
O:C	log([OA]/[BC])	-0.0345	0.407			0.17
H:C	log([OA]/[BC])	0.0228	1.737			0.27
$\log(MAC_{BrC,405nm})$	$\log(f_{ON\text{-}OA})$	0.322	0.446			0.33
$\log(MAC_{BrC,405nm})$	$\log(f_{ON\text{-}OA})$*	0.856	0.538			0.81
$\log(MAC_{BrC,405nm})$	f_{60}/f_{44}	-0.396	0.043			0.11
$\log(MAC_{BrC,405nm})$	f_{60}/f_{44}*	-2.242	0.803			0.96
log([ON]/[OA])	log([OA]/[BC])	-1.342	-0.320			0.47
log([ON]/[OA])	log([OA]/[BC])*	-1.342	-0.320			0.47
$k_{BrC,405nm}$	$MAC_{BrC,405nm}$	0.03104	-0.00177			0.99
$k_{BrC,532nm}$	$MAC_{BrC,532nm}$	0.0440	-0.00048			0.99

y	**x**	**c_1**	**c_2**	**c_3**	**c_4**	**r^2**
$w_{BrC,405\text{-}532}$	$AAE_{BrC,405\text{-}532}$	0.938	0.976			0.96
		$y = c_1 + c_2 \cdot \exp(-c_3 \cdot x)$				
MFR_{OA}	log([OA]/[BC])	0.00175	0.1760	0.8520		0.157

* Fits were performed to the Class averages, rather than to the individual burns.

Table S3. Literature imaginary refractive index and *MAC* values for biomass burning derived brown carbon.

	λ, nm	k_{BBOA}	MAC_{BBOA} m^2 g^{-1}	Optical Measurement	Aerosol type sampled	Sampling Location or note	Litera…
Laboratory	550	0.02-0.06		Aethalometer	Oak burning POA	-	(Saleh et a…
	550	0.015-0.04		Aethalometer	Pocosin Pine burning POA	-	(Saleh et a…
	550	0.0055-0.022		Aethalometer	Galberry burning POA	-	(Saleh et a…
	400	0.038	1.1	UV/Vis (filter methanol extracts)	Pine/Oak wood burning	-	(Chen and B…
	405	0.015		Photo-Acoustic Spectrometer	Tar balls from Ponderosa Pine Duff burning	-	(Chakrabarty…
	405	0.0076		Photo-Acoustic Spectrometer	Tar balls from Alaskan Duff burning	-	(Chakrabarty…
	550		0.8-3.2	CLAP	Tar balls from liquid tar (turkey oak)	-	(Hoffer et…
	405	0.01	0.35	Photo-Acoustic Spectrometer	Alaskan Peat	-	(Sumlin et…
	355, 405, 532, 1064	0.012, 0.0065, 0.0024, 0.0023		Photo-Acoustic Spectrometer	Alaskan & Indonesian Peat	central values reported here	(Sumlin et…
	600/400 ratio		0.04	Water soluble organic carbon	Florida peat	Ratio between wavelengths reported	(Sengupta e…
Ambient	404	0.01	1.0-1.1	Photo-Acoustic Spectrometer	Wild fire, near-source emission	Four Mile Canyon, Colorado	(Lack et a…
	470		1.01	Aethalometer	Biomass burning influenced	Beijing, China	(Yang et a…
	400	0.112	2.9	Filter transmission	Wood burning and biomass smoke aerosols	Savanna	(Kirchstetter…
	532	0.0016-0.0019	0.029-0.031	Photo-Acoustic Spectrometer	HULIS from biomass burning aerosols	Amazon basin	(Hoffer et…
	Broadband	0.05-0.07		Airborne lidar	Upwind of forest fires	Northern Canada	(Wandinger…
	Broadband	0.07±0.03/ 0.04±0.01		White light optical particle counter	Open fire/ Smoldering phase	Urban Rehovot, Israel	(Adler et a…
	405	0.037	0.79 or 1.22	Photo-Acoustic Spectrometer	Residential biomass burning influenced	Fresno, CA	(Zhang et…
	405		0.84	Photo-Acoustic Spectrometer	Residential biomass burning influenced	Fresno, CA	(Cappa et a…
	405		2.3	Aethelometer	Biomass burning influenced	Guangzhou, China	(Qin et a…
	365		0.32	Water soluble organic carbon	Plume intercept – closest point to fire	Western US	(Forrister et…
	365		1.35	Water soluble organic carbon	Regional biomass burning	SE US	(Washenfelde…

Formatted Table ... [1]
Deleted: 404
Deleted: 0.01
Deleted: 1.0-1.1
Deleted: Photo-Acoustic Spectrometer
Deleted: Four Mile Canyon, Colorado
Deleted: (Lack et al., 2012a)
Deleted: Wild fire, near-source emission
Deleted: 470
Deleted: 1.01
Deleted: Beijing, China
Deleted: (Yang et al., 2009)
Deleted: Aethalometer
Deleted: Biomass burning influenced
Deleted: 400
Deleted: Savanna
Deleted: (Kirchstetter et al., 2004)
Deleted: 0.112
Deleted: 2.9
Deleted: Filter transmission
Deleted: Wood burning and biomass smoke aerosols
Deleted: 532
Deleted: 0.0016-0.0019
Deleted: 0.029-0.031
Deleted: Photo-Acoustic Spectrometer
Deleted: (Hoffer et al., 2006)
Deleted: HULIS from biomass burning aerosols
Deleted: Amazon basin
Deleted: Broadband
Deleted: (Wandinger et al., 2002)
Deleted: 0.05-0.07
Deleted: Upwind of forest fires
Deleted: Northern Canada
Deleted: Airborne lidar
Deleted: Broadband
Deleted: 0.07±0.03/¶ ... [2]
Deleted: Urban Rehovot, Israel
Deleted: (Adler et al., 2011)
Deleted: White light optical particle counter
Deleted: Open fire/¶ ... [3]
Deleted: 405
Deleted: 0.037
Deleted: 0.79 or 1.22
Deleted: Fresno, CA
Deleted: (Zhang et al., 2016)
Deleted: Photo-Acoustic Spectrometer
Deleted: Residential biomass burning influenced
Deleted: 405
Deleted: 0.84
Deleted: Photo-Acoustic Spectrometer
Deleted: (Cappa et al., 2019b)
Deleted: Residential biomass burning influenced
Deleted: Fresno, CA
Deleted: 405
Deleted: 2.3
Deleted: Guangzhou, China
Deleted: (Qin et al., 2018)
Deleted: Aethelometer

405	0.037		Water soluble organic carbon	Regional	Kanpur, India	(Shamjad e
405		0.7-1.3	Water soluble organic carbon	Bonfire festival	Rehovot, Israel	(Bluvshtein
405		0.6	Methanol soluble organic carbon	Prescribed burn	NW US	(Xie et al
400, 600, 800	0.31, 0.26, 0.22		Electron loss	Asian outflow	Downwind of Asia	(Alexander e
800/400 ratio		0.26	Methanol soluble organic carbon	Ambient particles (ratio between wavelengths reported)	Athens, Georgia	(Phillips and
400, 550, 700	0.112, 0.030, 0.001		Acetone treatment + attenuation	African biomass burning	Southern Africa	(Kirchstetter

Deleted: 365

Deleted: 1.35

Deleted: Regional biomass burning

Deleted: SE US

Deleted: (Washenfelder et al., 2015)

Deleted: Water soluble organic carbon

Deleted: 405

Deleted: 0.037

Deleted: Regional

Deleted: Kanpur, India

Deleted: (Shamjad et al., 2016)

Deleted: Water soluble organic carbon

Deleted: 405

Deleted: 0.7-1.3

Deleted: Bonfire festival

Deleted: Rehovot, Israel

Deleted: (Bluvshtein et al., 2017)

Deleted: Water soluble organic carbon

Deleted: 0.6

Deleted: Methanol soluble organic carbon

Deleted: Prescribed burn

Deleted: (Xie et al., 2017)

Deleted: NW US

Deleted: 405

Deleted: {Alexander, 2008 #483}

Deleted: {Phillips, 2017 #2405}

Deleted: {Kirchstetter, 2004 #186}

Page 14: [1] Formatted Table	CDC	10/29/2019 10:14:00 AM

Formatted Table

Page 14: [2] Deleted	CDC	10/29/2019 10:12:00 AM

0.07±0.03/
0.04±0.01

Page 14: [3] Deleted	CDC	10/29/2019 10:12:00 AM

Open fire/
Smoldering phase